JEM Journal of Experimental Medicine

ARTICLE

Persistent RNA virus infection is short-lived at the single-cell level but leaves transcriptomic footprints

Peter Reuther[1*], Katrin Martin[1*], Mario Kreutzfeldt[2], Matias Ciancaglini[1], Florian Geier[3], Diego Calabrese[4], Doron Merkler[2], and Daniel D. Pinschewer[1]

Several RNA viruses can establish life-long persistent infection in mammalian hosts, but the fate of individual virus-infected cells remains undefined. Here we used Cre recombinase–encoding lymphocytic choriomeningitis virus to establish persistent infection in fluorescent cell fate reporter mice. Virus-infected hepatocytes underwent spontaneous noncytolytic viral clearance independently of type I or type II interferon signaling or adaptive immunity. Viral clearance was accompanied by persistent transcriptomic footprints related to proliferation and extracellular matrix remodeling, immune responses, and metabolism. Substantial overlap with persistent epigenetic alterations in HCV-cured patients suggested a universal RNA virus-induced transcriptomic footprint. Cell-intrinsic clearance occurred in cell culture, too, with sequential infection, reinfection cycles separated by a period of relative refractoriness to infection. Our study reveals that systemic persistence of a prototypic noncytolytic RNA virus depends on continuous spread and reinfection. Yet undefined cell-intrinsic mechanisms prevent viral persistence at the single-cell level but give way to profound transcriptomic alterations in virus-cleared cells.

Introduction

Viruses are commonly classified according to the fate of the infected host cell. Infections with cytolytic viruses eventually culminate in cell death. In contrast, noncytopathic/noncytolytic viruses such as hepatitis B and C virus (HBV, HCV) in humans and lymphocytic choriomeningitis virus (LCMV) in mice have developed strategies to avoid such a fatal outcome, supposedly with the aim of facilitating long-term persistence in their respective hosts. Members of the herpesvirus family as well as HBV and human papillomaviruses switch to a minimal viral gene expression program referred to as latent infection, maintaining their genomes as episomal DNA (Lieberman, 2016). In contrast, RNA viruses such as HCV or LCMV are thought to rely on continuously ongoing viral gene expression and RNA replication, thus bona fide "chronic infection" at the single-cell level. While the level of gene expression by these viruses may be tolerated by infected cells with only minimal detrimental effects, the antiviral immune response can also decide the fate of a virus-infected cell. CD8 T cells, for example, can eliminate virus-infected cells by cytotoxic mechanisms such as perforin and granzymes. Alternatively, CD8 T cells have been suggested to cleanse virus-infected cells by noncytolytic mechanisms, which prominently include IFN signaling (Binder and Griffin, 2001; Burdeinick-Kerr et al., 2009; Burdeinick-Kerr and Griffin, 2005; Guidotti et al., 1994; Guidotti et al., 1999a; Guidotti et al., 1996a; Guidotti et al., 1996b; Hausmann et al., 2005; Moseman et al., 2020; Oldstone et al., 1986; Parra et al., 1999; Patterson et al., 2002; Thimme et al., 2003; Tishon et al., 1993; Tishon et al., 1995). The latter mechanisms seem particularly important for irreplaceable cells such as neurons of the central nervous system (Binder and Griffin, 2001; Burdeinick-Kerr et al., 2009; Burdeinick-Kerr and Griffin, 2005; Griffin, 2010; Hausmann et al., 2005; Moseman et al., 2020; Oldstone et al., 1986; Parra et al., 1999; Patterson et al., 2002; Tishon et al., 1993) but have also been reported to play a prominent role in the clearance of persistently infected hepatocytes (Guidotti et al., 1994; Guidotti et al., 1999a; Guidotti et al., 1996a; Guidotti et al., 1996b; Guidotti et al., 1999b; Thimme et al., 2003). Interestingly, the survival of formerly virus-infected cells has even been reported for prototypic cytopathic viruses such as influenza A and B viruses (Chambers et al., 2019; Dumm et al., 2019; Hamilton et al., 2016; Heaton et al., 2014; Reuther et al., 2015). The underlying mechanisms, however, remain imperfectly understood. Also, these latter studies could not formally differentiate viral elimination after a period of active viral replication

[1]Department of Biomedicine, Division of Experimental Virology, University of Basel, Basel, Switzerland; [2]Department of Pathology and Immunology, Division of Clinical Pathology, Geneva Faculty of Medicine, Geneva University and University Hospital, Geneva, Switzerland; [3]Department of Biomedicine, Bioinformatics Core Facility, University Hospital Basel, Basel, Switzerland; [4]Department of Biomedicine, Histology Core Facility, University Hospital Basel, Basel, Switzerland.

*P. Reuther and K. Martin contributed equally to this paper; Correspondence to Daniel D. Pinschewer: daniel.pinschewer@unibas.ch.

from abortive infection events. Finally, potential long-term consequences of a transient viral infection on surviving cells and their progeny remain to be investigated.

For several decades, LCMV infection of mice, its natural host, has served as the prototypic model to study systemic persistent RNA virus infection, the impact of viral persistence on immunity, and the immunological mechanism implied in viral clearance (Hotchin, 1962; Traub, 1936; Volkert and Lundstedt, 1968; Zinkernagel, 2002). LCMV clearance in adult mice depends chiefly on antiviral CD8 T cells, with a significant contribution by antiviral antibodies when the course of the infection is protracted (Bergthaler et al., 2009; Fung-Leung et al., 1991). Neonatal infection, however, results in the negative selection of the antiviral CD8 T cell repertoire and lifelong persistence (Pircher et al., 1989; Traub, 1936). This coexistence of virus and host in a "carrier" state resembles in many aspects perinatally acquired human HBV infection (Guidotti and Chisari, 2001). In light of the noncytolytic nature of LCMV infection, it is widely assumed that in immunologically tolerant virus carriers, infected cells promote permanent viral gene expression and genome replication for their entire natural life span. However, long-standing observations on fluctuating viral titers in the supernatant of persistently infected cell cultures and a decrease of viral protein and RNA over time contrasted with this concept and stimulated the hypothesis that LCMV infection in cell culture is cyclic and transient (Hotchin, 1973a; Hotchin, 1973b; Hotchin, 1974; King et al., 2018; Lehmann-Grube, 1967; Oldstone and Buchmeier, 1982; Weber et al., 1983). Still, technical limitations have for the longest time precluded the fate mapping of LCMV-infected cells, notably in persistently infected mice.

Here, we have exploited a Cre recombinase (Cre) encoding LCMV (Steinbach et al., 2019) in conjunction with gene-targeted fate-reporter mouse models and cell lines to revisit the dogma of life-long viral persistence at the single-cell level. We found that even in highly immune-deficient mice, LCMV cannot efficiently persist at the single-cell level but relies on continuous spread in order to maintain the infection. Clearance at the single-cell level was observed in the absence of adaptive immunity and independently of type I or type II IFN signaling, and was accompanied by profound transcriptome alterations.

Results

Non-cytolytic viral clearance from hepatocytes of congenitally infected carrier mice

To elucidate the fate of LCMV-infected cells in various experimental systems, we relied on genetically engineered cell fate reporter models. $STOP_{flox}$-RFP mice, for example, carry an RFP transgene in the ubiquitously active ROSA26 locus, preceded by a loxP-flanked transcription termination sequence. Cre-mediated loxP site recombination upon infection by a Cre-expressing LCMV ($artLCMV_{Cre}$) allows for cellular fate mapping based on the irreversible activation of RFP expression in the infected cell and its progeny. $artLCMV_{Cre}$ encodes for Cre in a way that allows neither its immediate translation nor direct Cre mRNA transcription (Fig. S1, A and C). Rather, Cre expression and reporter gene trans-activation depend on full-length viral genome replication followed by mRNA transcription from the resulting antigenomic template. Experiments conducted in a Cre-reporting A549 cell line confirmed that viral particles delivering Cre failed to trans-activate fluorescent reporter activity unless the viral polymerase replicated the incoming viral genome into a viral antigenome and from this template transcribed viral Cre mRNA (Fig. S1, B and D). These studies validated $artLCMV_{Cre}$-induced fluorescence as a readout of current or past active viral genome replication, thus excluding abortive infection by replication-incompetent, defective viral particles as a potential confounder in our cellular fate mapping analyses.

To determine the fate of LCMV-infected primary hepatocytes in culture, we prepared single-cell suspensions from the liver of RFP fate reporter mice ($STOP_{flox}$-RFP) and infected them with $artLCMV_{Cre}$ (Fig. 1 A and Fig. S1 H). 2 d later, the majority of hepatocytes expressed the viral nucleoprotein (NP) but had not yet accumulated detectable levels of RFP, a stage of infection subsequently referred to as "early infected." By day 6 to day 8, virtually the entire culture expressed NP and had accumulated clearly detectable levels of RFP, a stage of infection herein referred to as "late infected." Intriguingly, when following the culture for 13 or even 16 d, a substantial proportion of hepatocytes (~20–60%) no longer expressed detectable levels of NP yet were clearly RFP-positive. This pattern (NP^-RFP^+) suggested that the respective cells had cleared $artLCMV_{Cre}$ infection in a noncytolytic, hepatocyte-intrinsic manner. An inherent limitation of this $artLCMV_{Cre}$-based fate mapping approach consists, however, in the inability to discriminate between formerly infected, virus-cleared cells and the progeny of such cells. For simplicity, both types of cells will be referred to as "cleared" throughout this study. Similar to the above findings with $artLCMV_{Cre}$, the percentage of NP-expressing (infected) primary hepatocytes increased from day 2 to day 6 after WT LCMV infection but declined continuously at later time points (Fig. S1 G).

While our primary hepatocyte cultures remained viable for 16 d (Fig. S1 H), transcriptional changes upon long-term ex vivo culture have been reported and may reflect cellular dedifferentiation (Clayton and Darnell, 1983), with a currently unknown impact on viral persistence. Neonatal infection of mice with WT LCMV results in an immunologically tolerant carrier state (Cole et al., 1972; Hotchin, 1962; Traub, 1936). Here, we infected neonatal $STOP_{flox}$-RFP mice with $artLCMV_{Cre}$ to test whether infected hepatocytes can undergo noncytolytic clearance in living animals. As expected, $artLCMV_{Cre}$ established a systemic carrier state, which was evident in high levels of viral RNA in liver, lung, spleen, and brain at 3 wk of age, and infectious virus was detectable in blood (viremia), spleen, and lung for up to 20 wk (Fig. 1, B and C; and Fig. S2, A–D). In remarkable contrast, infection of adult mice with $artLCMV_{Cre}$ did not result in viremia, and viral loads were only transiently detected in spleen and liver on day 4 after infection but were suppressed to undetectable levels by day 8 (Fig. S2, E–H). Immunohistochemical analyses demonstrated that $artLCMV_{Cre}$ replication in the liver of adult infected animals was restricted to Kupffer cells, the first target of LCMV infection in this organ (Bergthaler et al., 2007), and was cleared before significant spread into hepatocytes occurred (Fig. S2 I). This limitation precluded the study

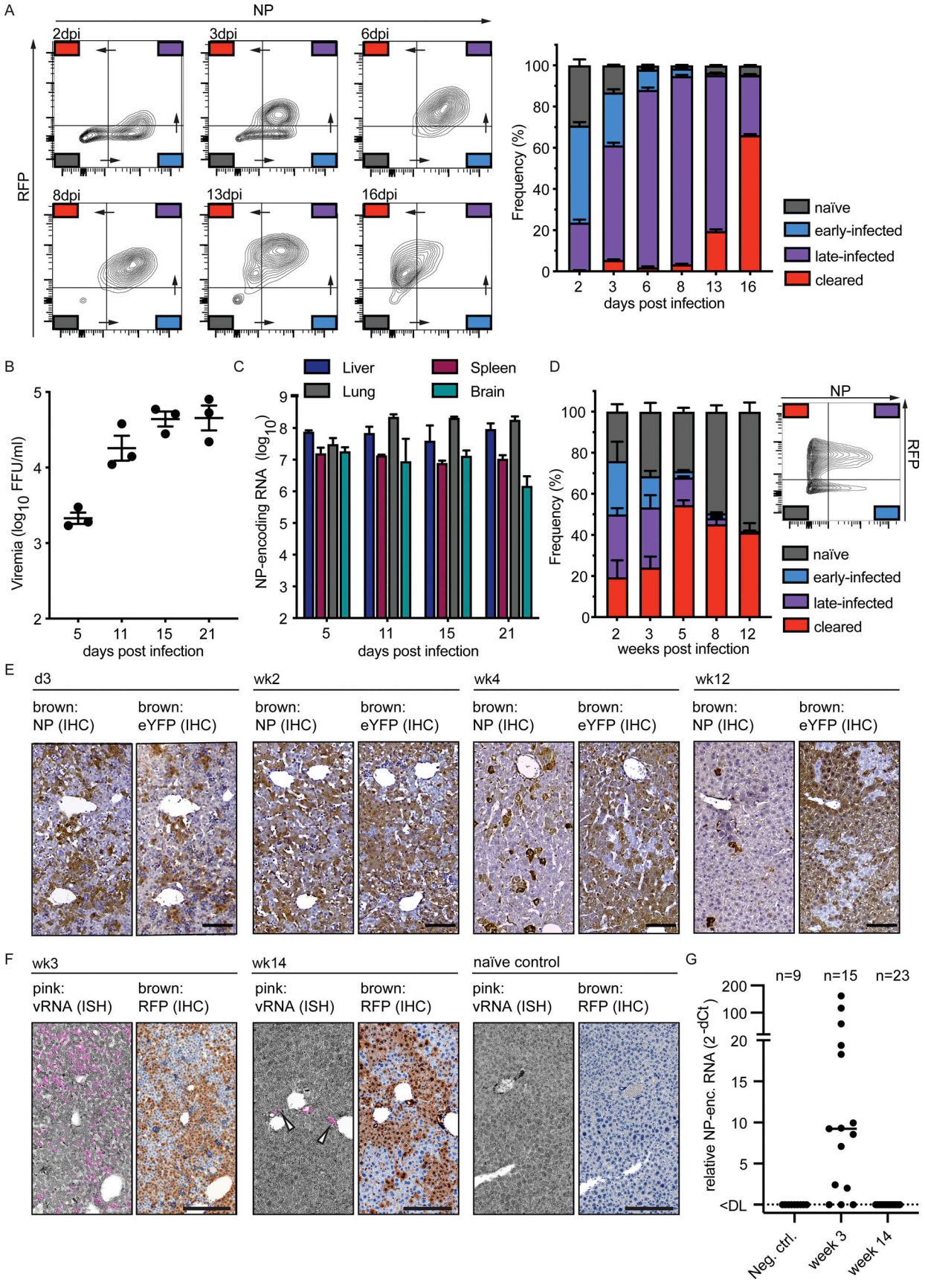

Figure 1. **LCMV-infected hepatocytes are cleared in a noncytolytic manner. (A)** We isolated and cultured primary hepatocytes of $STOP_{flox}RFP$ mice. At the indicated time points after infection with $artLCMV_{Cre}$ (MOI = 0.025), we analyzed viral NP and RFP expression. Representative FACS plots of three replicate

cultures are shown. Stacked bars depict the average frequencies of cells falling into the respective gates. The gating strategy used for the analysis of murine hepatocytes is exemplified in Fig. S2 A. Total numbers of primary hepatocytes and their viability are displayed in Fig. S2 D. **(B and C)** Viral titer in blood (B) and NP-encoding RNA copies per 100 ng total RNA in liver, spleen, lung, and brain (C) of $STOP_{flox}$RFP mice neonatally infected with $artLCMV_{Cre}$. **(D)** Flow-cytometric analysis of viral NP and RFP expression in hepatocytes isolated from $STOP_{flox}$RFP mice at the indicated time points after neonatal $artLCMV_{Cre}$ infection. One representative FACS plot out of three animals analyzed at week 5 is shown. Stacked bars depict the average frequencies of cells falling into the respective gates. The gating strategy is exemplified in Fig. S2 A. **(E)** Immunohistochemical analysis of NP and eYFP expression in liver sections of $STOP_{flox}$eYFP mice neonatally infected with $artLCMV_{Cre}$ (scale bar, 100 µm). Representative images from one out of three animals are shown. An immunofluorescent costaining of NP and eYFP is depicted in Fig. S2 B. **(F)** Visualization of RFP (brown) and viral genomic RNA (vRNA, pink) by immunohistochemistry (IHC) and in situ hybridization (ISH), respectively, in sequential liver sections from $STOP_{flox}$RFP mice neonatally infected with $artLCMV_{Cre}$. Arrowheads point out select vRNA-positive cells (scale bar, 100 µm). Representative images from three animals are shown. **(G)** We infected neonatal $STOP_{flox}$RFP mice with $artLCMV_{Cre}$ and single-cell–sorted RFP-positive hepatocytes at weeks 3 and 14. Levels of viral NP-encoding RNA in individual cells were normalized to GAPDH for display. Single-cell–sorted hepatocytes from an uninfected animal served as negative control. Symbols in B and G represent individual mice and cells, respectively. Error bars indicate SEM. Number of biological replicates, $n = 3$ (A–C), $n = 3$ (D; week 2–8), $n = 4$ (D, week 12). Representative data from two similar, independently conducted experiments are shown (A–E and G). 1 representative out of 23 visual fields from a total of 4 mice is shown (F). ctrl., control; DL, detection limit; enc., encoding; FFU, focus forming units; Neg., negative.

of $artLCMV_{Cre}$ clearance from hepatocytes in adult infected mice such that all further in vivo studies were conducted in neonatally infected animals. We isolated hepatocytes for flow cytometric analysis at week 2 after neonatal infection and found that ∼40% of all hepatocytes were actively infected as judged by NP expression (Fig. 1 D and Fig. S1 E). Of note, half of these cells expressed NP but had not yet accumulated detectable levels of RFP, and thus were early infected, while the other half were late-infected cells expressing both NP and RFP. Analogous to the above findings in cell culture, another 20% of hepatocytes in carrier mice reported Cre-induced RFP but were negative for the NP, indicating that these cells were cleared, i.e., had been infected by $artLCMV_{Cre}$ but were no longer actively infected at the time point of analysis. By week 5 after neonatal infection, about half of the liver consisted of cleared hepatocytes, and such cells still made up for >40% at weeks 8 and 12 (Fig. 1 D). The proportion of actively infected cells (sum of early infected and late infected), however, decreased considerably over time and by week 12 after neonatal infection accounted for <1% of all hepatocytes. In a complementary approach, we analyzed non-cytolytic $artLCMV_{Cre}$ clearance on histological liver sections of enhanced YFP (eYFP) fate reporter mice ($STOP_{flox}$-eYFP). Immunostaining for viral NP revealed that infection of the liver emanated from numerous foci of infected cells, which were present on day 3 and spread through the entire organ by week 2, at which point a majority of hepatocytes expressed NP (Fig. 1 E; and Fig. S1, F and J). In contrast, at week 4 and similarly at week 12 after neonatal infection, only a comparably low number of infected (NP-positive) hepatocytes was loosely scattered throughout the tissue. On day 3 and at week 2, Cre-induced eYFP expression matched the abundance of NP-positive cells, whereas at week 4 and at week 12, $eYFP^+$ cells outnumbered NP^+ cells by far. This finding was in line with our flow cytometry–based analysis (Fig. 1 E, compare Fig. 1 D), indicating that a substantial proportion of hepatocytes had undergone noncytolytic viral clearance. Likewise, we detected noncytolytically cleared cells in lung, kidney, and ileum of $STOP_{flox}$-RFP mice at week 12 after infection (Fig. S1 I). Next, we investigated whether hepatocytes judged as cleared based on the lack of detectable viral NP were thoroughly cleansed from viral genomes. We performed single molecule in situ hybridization (Calabrese and Wieland, 2017) to detect $artLCMV_{Cre}$ genomic RNA on liver sections from $artLCMV_{Cre}$-infected $STOP_{flox}$-RFP mice (Fig. 1 F and Fig. S1 K). A large proportion of cells, mostly hepatocytes, contained viral genomic RNA at week 3 after infection, whereas only very few randomly scattered cells still harbored LCMV RNA at week 14. The latter finding contrasted, again, with the vast number of cells that expressed recombination-induced RFP (Fig. 1 F). To corroborate these conclusions, we performed single-cell RT-qPCR (quantitative RT-PCR) on RFP-positive hepatocytes. Whereas most of the cells collected at week 3 after neonatal infection contained $artLCMV_{Cre}$ RNA, the cells recovered at week 14 were virus-free (Fig. 1 G). Next, we investigated whether the population of cleared hepatocytes persisting at late time points after neonatal infection (compare Fig. 1 D) represented individual cellular infection events or rather clonally expanding populations of formerly infected cells. For this we exploited R26R-Confetti mice (Livet et al., 2007), which upon Cre-recombination stochastically express one out of four fluorescent proteins (Fig. S3 A). At week 12 after neonatal infection, these four fluorescent labels were randomly interspersed throughout the liver of neonatally infected animals (Fig. S3 B), indicating that even clusters of Cre-recombined hepatocytes originated from several distinct infection and recombination events. Taken together, these findings argued against a prominent clonal expansion of formerly infected cells and demonstrated that a substantial proportion of formerly infected hepatocytes had undergone noncytolytic viral clearance and populated the liver of carrier mice.

Non-cytolytic $LCMV_{Cre}$ clearance occurs independently of T cells, B cells, and type I or type II IFN signaling

The frequency of actively $artLCMV_{Cre}$-infected hepatocytes decreased from about week 4 after neonatal infection onwards (Fig. 1, D–F), and viremia in $STOP_{flox}$-RFP mice also declined considerably (Fig. 2 A). This partial virus control coincided with the maturation of the murine adaptive immune system (Siegrist, 2001), prompting us to investigate a potential role of adaptive immunity in noncytolytic virus clearance from hepatocytes of $STOP_{flox}$-RFP mice. Unlike immunocompetent $STOP_{flox}$-RFP mice, Rag1-deficient $STOP_{flox}$-RFP mice (Rag1 × $STOP_{flox}$-RFP), devoid of T and B cells, remained highly viremic throughout the 12-wk observation period (Fig. 2 A), and a substantial proportion

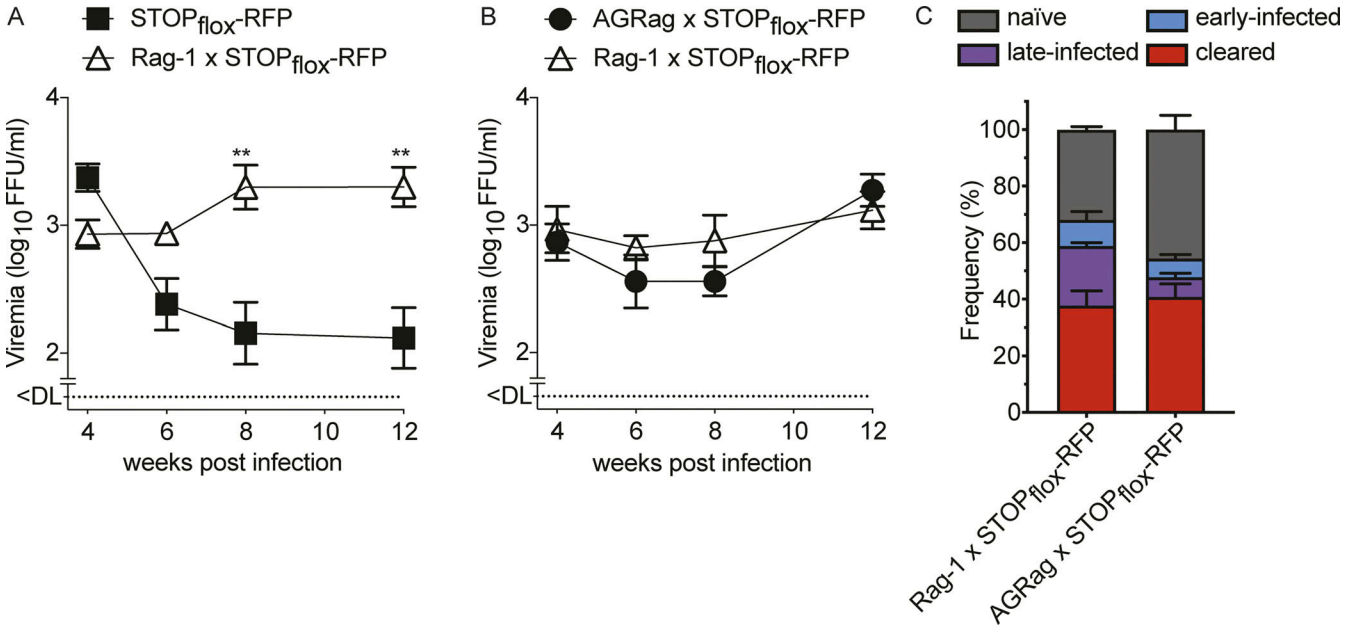

Figure 2. **Non-cytolytic clearance occurs independently of adaptive immunity and independently of type I or type II IFN signaling. (A and B)** Viremia of $STOP_{flox}$RFP mice (A), Rag-1 × $STOP_{flox}$RFP mice (A and B), and AGRag × $STOP_{flox}$RFP mice (B) neonatally infected with $artLCMV_{Cre}$. **(C)** Flow-cytometric quantification of NP expression and RFP expression in hepatocytes from Rag-1 × $STOP_{flox}$RFP mice or AGRag × $STOP_{flox}$RFP mice at week 5 after neonatal infection with $artLCMV_{Cre}$. Bars reflect average frequencies (%) of cells that fall into the respective gates. Error bars represent SEM. Number of biological replicates, $n = 7$ ($STOP_{flox}$RFP), $n = 4$ (Rag-1 × $STOP_{flox}$RFP; A), $n = 6$ (Rag-1 × $STOP_{flox}$RFP), $n = 4$ (AGRag × $STOP_{flox}$RFP; B), $n = 3$ (Rag-1 × $STOP_{flox}$RFP), $n = 4$ (AGRag × $STOP_{flox}$RFP; C). Representative data from two similar, independently conducted experiments are shown (A–C). Two-way ANOVA with Bonferroni's post-test was used for multiple comparisons. **, $P < 0.01$. DL, detection limit; FFU, focus forming units.

(~25%) of the animals' hepatocytes evidenced active viral replication at 12 wk of age (Fig. 2 C). This indicated that systemic control of congenital $artLCMV_{Cre}$ infection relied on adaptive immune mechanisms. Even in the absence of T and/or B cell–mediated virus control, however, the liver of Rag1 × $STOP_{flox}$-RFP mice harbored ~40% noncytolytically cleared (NP^-RFP^+) hepatocytes (Fig. 2 C and Fig. S3 C). While the availability of antiviral T and B cells in WT mice is likely to influence the relative contribution of noncytolytic clearance to virus control in tissues, the present findings demonstrated that noncytolytic clearance can occur independently of the adaptive immune system. Type I (α/β) IFNs as well as T cell–secreted type II IFN (IFN-γ) have been described as key effector pathways in noncytolytic hepatocyte clearance, while type III IFN (IFN-λ) cannot be sensed by murine hepatocytes (Guidotti et al., 1996a; Guidotti et al., 1996b; Hermant et al., 2014). To explore a potential role of type I and/or type II IFN signaling in noncytolytic $LCMV_{Cre}$ clearance, and to also address these pathways' potential redundancy with adaptive immunity, we studied $STOP_{flox}$-RFP mice devoid of T and B cells (RAG1-deficient) and, additionally, devoid of functional type I and type II IFN receptors (AGRag [type I IFN receptor–, type II IFN receptor–, and RAG-1–deficient] × $STOP_{flox}$-RFP). Analogous to Rag1 × $STOP_{flox}$-RFP mice, neonatally $artLCMV_{Cre}$-infected AGRag × $STOP_{flox}$-RFP mice remained highly viremic throughout the observation period of 12 wk. Intriguingly, even in these highly immunodeficient mice, 40% of all hepatocytes were NP^-RFP^+, thus noncytolytically cleared. These findings demonstrated that noncytolytic $artLCMV_{Cre}$ clearance from hepatocytes can occur in the absence of T cells and B cells even when, in addition, type I and type II IFN sensing is disabled (Fig. 2, B and C).

Viral persistence depends on continuous viral spread and reinfection

To investigate whether noncytolytic clearance occurs also in immortalized cell lines, we infected Cre-reporting, human lung–derived A549 cells ($A549_{floxGFP}$) with $artLCMV_{Cre}$. After 3 d, the culture consisted mostly of NP-expressing and Cre-recombined (GFP^+) late-infected cells. Over the subsequent days, the NP signal faded continuously until at around day 11, the vast majority of cells (~97%), albeit almost uniformly expressing GFP, had become NP negative. This indicated viral clearance after a period of active viral replication and Cre expression. By day 14, however, the virus reemerged, and most cells were again NP^+, resulting in a wave-like pattern of NP expression over time (Fig. 3 A; and Fig. S4, A and C). Irrespective of potential confounders such as cell culture splitting and accompanying culture medium exchange, this observation lent further support to the hypothesis that LCMV does not persist at the single-cell level but relies on continuous spread or, notably in the case of cell cultures, reinfection of formerly infected cells or their progeny. To test this postulate, we infected $A549_{floxGFP}$ cells with a viral glycoprotein (GP)–deficient but GP protein pseudotyped, Cre-encoding LCMV ($LCMV\Delta GP_{Cre}$). Such viral particles can enter cells to amplify and express their genetic information but they cannot spread in the culture since they are unable produce infectious progeny particles (Flatz et al., 2010). NP expression peaked 1 d after infection (at multiplicity of infection [MOI] of

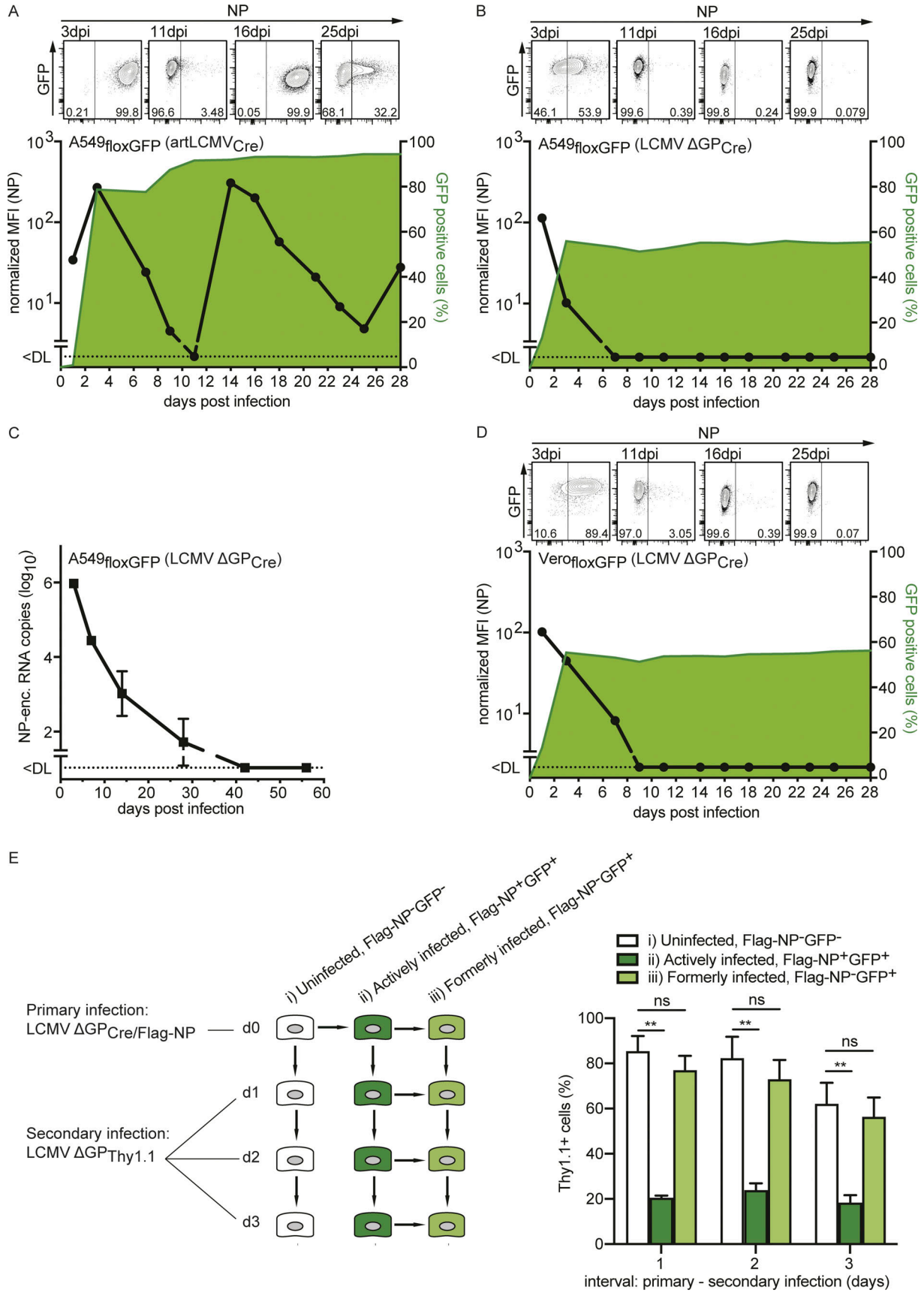

Figure 3. **LCMV is cleared from cultured cells and persistence depends on viral spread. (A, B, and D)** Analysis of viral NP and GFP expression by $A549_{floxGFP}$ cells (A and B) and $Vero_{floxGFP}$ cells (D) infected with $artLCMV_{Cre}$ (MOI = 0.01; A) or $LCMV\Delta GP_{Cre}$ (MOI = 0.5; B and D). Small contour plots above

each main graph illustrate NP expression levels in the GFP-positive cell population at the indicated time points. Numbers within the plots indicate percentages of NP-negative cells (left gates) and NP-positive cells (right gates). To monitor absolute levels of viral NP over time (left y axis; NP mean fluorescence intensity [MFI] of GFP-positive cells is shown), its MFI was normalized to a standard included in each measurement (LCMVΔGP$_{Cre}$-infected control cells [A549$_{floxGFP}$] at 48 h after infection). The frequency (%) of GFP-expressing cells is indicated as a green shaded area (right y axis). The gating strategy is exemplified in Fig. S3 A. **(C)** Average number of NP-encoding RNA copies per 100 ng total RNA of LCMVΔGP$_{Cre}$-infected A549$_{floxGFP}$ cells. **(E)** Schematic representation of the superinfection exclusion experiment (left). A549$_{floxGFP}$ cultures were subject to primary infection with LCMVΔGP$_{Cre/Flag\text{-}NP}$ at MOI = 0.5. After infection (uninfected cells [i] displayed in white), the cells start expressing GFP. The initial phase of active infection (ii) can be identified by the presence of both GFP and the (flag-tagged) NP (dark green in schematic, Flag-NP$^+$), whereas formerly infected but cleared cells (iii, light green in schematic, Flag-NP$^-$) express only GFP. At the indicated interval after primary infection (1 d, 2 d, 3 d), the cultures were subject to secondary infection with LCMVΔGP$_{Thy1.1}$ at MOI = 1. Thy1.1 expression in the three aforementioned cell populations (white, dark green, light green) was determined by flow cytometry (right) 24 h after secondary infection. Bar graphs depict average frequencies of Thy1.1-expressing cells. Error bars indicate SD (n = 3). Unpaired two-tailed Student's t test was used for pairwise comparisons. **, P < 0.01. The gating strategy is exemplified in Fig. S3 B. Representative data from two similar, independently conducted experiments are shown (C and E). Contour plots and xy plots are representative of six replicates (A, B, and D). DL, detection limit; dpi, days post-infection; enc., encoding.

~0.5), and from day 3 onwards, the culture contained ~60% of GFP-positive Cre-reporting cells (Fig. 3 B and Fig. S4 D). NP levels, however, declined sharply from d 1 onwards and reached detection limits of flow cytometry by day 7. Importantly and in contrast to artLCMV$_{Cre}$ infection (Fig. 3 A and Fig. S4 C), NP remained undetectable throughout day 28, indicating that artLCMV$_{Cre}$ persistence in cell culture relies on continuous (GP dependent) reinfection cycles of formerly infected and transiently cleared cells and/or infection of their progeny. Accordingly, intracellular viral RNA in LCMVΔGP$_{Cre}$-infected A549$_{floxGFP}$ cells reached an early peak, then declined rapidly. It fell below detection limits of TaqMan RT-PCR by day 42 after infection and did not reemerge until day 57, suggesting that LCMVΔGP$_{Cre}$ had been eliminated from the culture because it failed to propagate (Fig. 3 C). In line with the observation that the proportion of formerly LCMVΔGP$_{Cre}$-infected and therefore Cre-recombined (GFP$^+$) cells remained constant from day 3 until day 28 (Fig. 3 B and Fig. S4 D), these GFP$^+$ cells exhibited unimpaired viability and divided at a rate that was indistinguishable from virus-naive cells in the same culture (Fig. S4, F–H). The above studies in AGRag × STOP$_{flox}$-RFP mice had indicated that type I IFN signaling was dispensable for noncytolytic viral clearance. To corroborate these conclusions and extend them to cell culture, we performed LCMVΔGP$_{Cre}$ infection experiments in Cre-reporting Vero cells (Vero$_{floxGFP}$), a cell type known to be type I IFN–deficient (Desmyter et al., 1968; Mosca and Pitha, 1986; Fig. 3 D and Fig. S4 E). Viral NP expression peaked on day 1 but subsided to below detection limits by day 9 after infection, indicating that type I IFN–dependent mechanisms were not accountable for clearance from cell culture.

The wave-like pattern of viral clearance and subsequent reinfection in artLCMV$_{Cre}$-infected cultures (Fig. 3 A and Fig. S4 C) suggested that viral infection and clearance was accompanied by a refractory period, i.e., a time window during which infected or recently cleared cells were insusceptible to superinfection or reinfection, respectively. To test this hypothesis, we infected A549$_{floxGFP}$ cultures with a LCMVΔGP$_{Cre}$ virus carrying a Flag-tagged NP (LCMVΔGP$_{Cre/Flag\text{-}NP}$). Upon infection at MOI of ~0.5, we differentiated three subsets of cells in the cultures. Besides (i) a population of uninfected, nonrecombined cells (Flag-NP$^-$GFP$^-$; Fig. 3 E and Fig. S4 B), the viral Flag-tag allowed us to differentiate Cre-recombined (GFP$^+$) cells, which were either (ii) actively infected, nucleoprotein-expressing (Flag-NP$^+$GFP$^+$) cells or (iii) formerly infected cells that had cleared LCMVΔGP$_{Cre/Flag\text{-}NP}$-infection (Flag-NP$^-$GFP$^+$; Fig. 3 E). At various time points after LCMVΔGP$_{Cre/Flag\text{-}NP}$ "primary" infection, we exposed the cultures to "secondary" infection with a GP-deficient LCMV devoid of a Flag-tag but encoding for the cell surface–expressed Thy1.1 marker (LCMVΔGP$_{Thy1.1}$). The percentage of Thy1.1-expressing cells among the three aforementioned populations (i, ii, and iii) allowed us to determine the respective cells' susceptibility to infection or superinfection, respectively. As expected, the proportion of Flag-NP$^+$ cells declined continuously from day 1 onwards (data not shown). Independently thereof, nucleoprotein-expressing cells (ii) were, on average, four times less permissive to LCMV infection than not previously infected cells (i) or cells that had cleared LCMVΔGP (iii; Fig. 3 E). It remains unknown whether this result reflects only partial refractoriness during infection or, more likely, that the iii subset of cells consisted of some completely refractory cells and other partially or fully permissive cells, perhaps as a function of time elapsed after viral clearance. Still, this result was in line with the concept that active viral replication rendered cells refractory to superinfection (Damonte et al., 1983; Welsh and Pfau, 1972), a phenomenon also referred to as "superinfection exclusion" (Ellenberg et al., 2004) that likely accounted for the wave-like pattern of artLCMV$_{Cre}$ infection in cell culture (Fig. 3 A). Two additional points are of note. First, "refractoriness" to LCMV infection was observed for cell populations growing in the midst of fully susceptible cells, suggesting that refractoriness was cell-intrinsic and not transmissible from one cell to the next. Second, Cre-recombined cells undergoing noncytolytic clearance reacquired, eventually, unimpaired susceptibility to LCMV (re) infection.

Non-cytolytic clearance occurs independently of the viral Z protein

The viral matrix protein Z has been shown to inhibit viral RNA transcription and replication when present at high intracellular concentrations, supposedly by favoring viral genome packaging into budding particles (Cornu and de la Torre, 2001; Kranzusch and Whelan, 2011). It was therefore tempting to speculate that the viral Z protein mediated noncytolytic viral clearance. To test this hypothesis, we generated an LCMV-expressing Cre in lieu of the Z gene (LCMVΔZ$_{Cre}$). LCMVΔZ$_{Cre}$ was strictly cell-associated and spread only slowly through A549$_{floxGFP}$ cultures (Fig. 4 A). By day 45, only ~50% of the cells had encountered the virus as evident by Cre-induced GFP expression. Intriguingly, though,

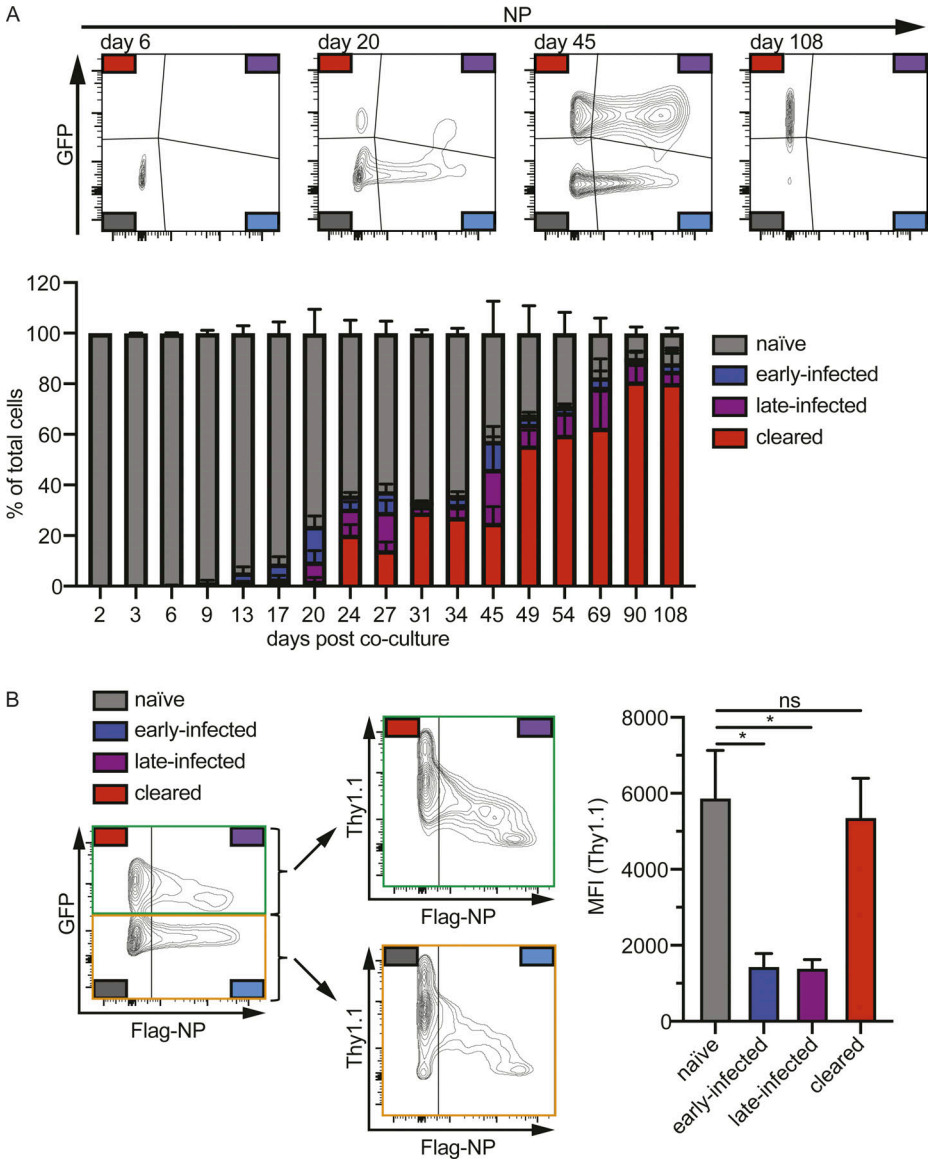

Figure 4. **Non-cytolytic clearance and superinfection exclusion occur independently of the viral Z protein. (A)** Flow-cytometric analysis of viral NP and GFP expression by $A549_{floxGFP}$ cells at the indicated time points after primary infection with $LCMV\Delta Z_{Cre}$ (see Materials and methods for details). FACS plots are representative of three replicate cultures. Stacked bars depict the average frequencies of cells that fall into the respective gates. **(B)** $A549_{floxGFP}$ cells were infected with $LCMV\Delta Z_{Cre/Flag\text{-}NP}$. When ∼25% of the cells were Flag-positive (day 105 after co-culture), they were superinfected with $LCMV\Delta GP_{Thy1.1}$ (MOI = 1). We compared Thy1.1 expression levels in actively $LCMV\Delta Z_{Cre/Flag\text{-}NP}$-infected ($NP\text{-}Flag^+$, early and late infected) and not actively infected ($NP\text{-}Flag^-$, naive, and cleared) cells in the same culture 24 h after superinfection. One representative FACS plot out of three independent cultures is displayed. The bar graph displays the Thy1.1 mean fluorescent intensity (MFI). Error bars plot SD (n = 3). Paired two-tailed Student's t test was used for pairwise comparisons. *, $P < 0.05$. Representative data from two similar, independently conducted experiments are shown (A and B).

more than half of these Cre-recombined cells contained undetectable levels of viral NP, indicating that noncytolytic clearance had occurred in the absence of the viral Z protein. By day 108, the vast majority of cells had been infected (GFP^+) but had cleared the virus (NP^-). To investigate whether the viral Z protein is accountable for superinfection exclusion as previously postulated (Cornu et al., 2004), we generated a Z-deficient, Cre-encoding LCMV with a flag-tagged NP ($LCMV\Delta Z_{Cre/Flag\text{-}NP}$). We tested whether $A549_{floxGFP}$ cells, when infected with $LCMV\Delta Z_{Cre/Flag\text{-}NP}$, remained permissive to $LCMV\Delta GP_{Thy1.1}$. On the contrary, Thy1.1 levels in NP-Flag–positive cells ($LCMV\Delta Z_{Cre/Flag\text{-}NP}$-infected, early or late infected) were substantially lower than in NP-Flag–negative cells (naive or cleared), indicating that Z protein expression was not or at least not fully accountable for superinfection exclusion (Fig. 4 B). Again, cells that had cleared the infection were as susceptible to infection as naive cells from the same culture.

Transcriptome signature of noncytolytic viral clearance from hepatocytes

Cell-intrinsic elimination of $artLCMV_{Cre}$ with a refractory period and resistance to superinfection suggested changes in

cellular homeostasis. Hence, we set out to investigate whether formerly infected but cleared cells exhibited transcriptomic alterations. To this end, we collected hepatocytes from 14-wk-old $STOP_{flox}$-RFP mice that had been neonatally infected with $artLCMV_{Cre}$ ("carriers"). Hepatocytes were sorted according to RFP expression, and total cellular RNA of each population was subject to bulk mRNA sequencing (mRNA-Seq). Importantly, the proportion of actively infected hepatocytes was <1% at 14 wk after infection (Fig. 1 D and data not shown), such that RFP-negative hepatocytes consisted virtually exclusively of uninfected cells while RFP-positive hepatocytes were almost exclusively formerly infected, cleared cells. To account for potential transcriptome alterations as a result of RFP expression, not only hepatocytes from uninfected $STOP_{flox}$-RFP mice but also RFP-reporting hepatocytes from uninfected mice with liver-specific RFP expression ($STOP_{flox}$-RFP × Alb-Cre) were included as controls. Strikingly, the transcriptomes of noncytolytically cleared hepatocytes from six individual animals clustered together and were clearly differentiated from both, the RFP-negative hepatocytes of the same animals as well as from hepatocytes of the aforementioned uninfected control groups (Fig. 5 A). In noncytolytically cleared hepatocytes, 1,272 genes were significantly up-regulated as compared with uninfected cells from the same animals (Fig. 5 B). The transcriptome of the latter cells was more similar to hepatocytes of uninfected $STOP_{flox}$-RFP mice (271 differentially expressed genes; Fig. 5, A and B). Hepatocytes of uninfected $STOP_{flox}$-RFP mice differed only marginally from those of $STOP_{flox}$-RFP × Alb-Cre mice, excluding RFP expression as an important source of transcriptomic alterations. Altogether, this indicated that most of the transcriptome alterations in noncytolytically cleared hepatocytes had occurred in a cell-intrinsic manner rather than in a bystander fashion. Virus-cleared hepatocytes exhibited a prominent enrichment of gene sets and pathways related to (1) immune responses, (2) cell metabolism, and (3) proliferation and extracellular matrix remodeling (Fig. 5 C). Up-regulation of the latter may indicate a response to cellular stress and/or damage triggered as a consequence of the viral infection. In contrast, pathways involved in metabolic functions were negatively enriched. To identify transcription factors (TFs) supposedly driving these gene expression alterations, we employed a regulon analysis (Garcia-Alonso et al., 2019; Holland et al., 2020) focused on high-confidence TF–target gene relationships and limited to TFs detectable in our mRNA-Seq dataset. This analysis yielded seven factors, three of which were up-regulated in noncytolytically cleared hepatocytes: Spi1/PU.1, Erg, and Tal1 (Fig. 5 D and Fig. S5 A). Spi1/PU.1, our top hit, is a key regulator of pro-fibrotic gene expression (Wohlfahrt et al., 2019) and was up-regulated 13-fold. In contrast, Erg expression is known to counteract liver fibrogenesis (Dufton et al., 2017) and itself is a target of Tal1 (Thoms et al., 2011; Fig. 5 D). We performed TaqMan RT-PCR to validate genes of interest, which mRNA-Seq had suggested were differentially expressed in noncytolytically cleared hepatocytes (RFP^+) and uninfected (RFP^-) hepatocytes of carrier mice (Fig. S5 B). Finally, we investigated whether the transcriptomic footprint of LCMV clearance reflected, at least in part, a universal hepatocytic response to transient RNA virus infection. We compared our mRNA-Seq data to published genome-wide ChIPmentation-based chromatin immunoprecipitation DNA-sequencing datasets on human liver biopsies from HCV patients, either chronically infected or cleared by direct-acting antiviral (DAA) treatment (Fig. 5 E; and Fig. S5, C and D; Boldanova et al., 2017; Hamdane et al., 2019). Strikingly, for 82% of the genes, which we found up-regulated in formerly LCMV-infected mouse hepatocytes (Log_2 [FC]>1), the human orthologs in DAA-cured subjects were characterized by H3K27ac modifications (Log_2[FC]>0; Fig. 5 E and Table S1). Analogous results were also obtained for a second independent cohort of DAA-cured HCV patients as well as for chronically HCV-infected patients (Fig. S5, C and D; and Table S1), and the relatedness of transcriptomic signatures was also validated by comparison to human RNA sequencing data (Fig. S5, E and F). These observations indicated that the transcriptomic footprint of cleared infection exhibited a substantial degree of conservation across different mammalian species and distantly related RNA viruses.

Discussion

This study redefines LCMV persistence as a dynamic process, which depends on continuous viral spread; meanwhile, individual infected cells undergo cell-intrinsic noncytolytic clearance.

These conclusions are compatible with observations from other infections suggesting the viral persistence strategy described herein is not unique to the arenavirus family. Antibody-mediated elimination of HCV infection in human liver chimeric mice, for example, has demonstrated that HCV needs to continuously infect new hepatocytes to sustain a chronic infection (de Jong et al., 2014). Analogously, the entry inhibitor Hepcludex can reduce intracellular loads of hepatitis D virus and HBV genomes (Allweiss et al., 2018; Bogomolov et al., 2016). Henceforth, the demonstration of noncytolytic clearance at the single-cell level, a process occurring in a cell-intrinsic manner even when adaptive immunity and IFN signaling are disabled, provides a new mechanistic incentive for the use of entry inhibitors in the treatment of persistent RNA virus infections.

One consequence of this new concept of RNA virus persistence consists of permissive organs such as the liver harboring a substantial proportion of formerly virus-infected cells. Our transcriptome data indicate that cellular homeostasis remains perturbed beyond the viruses' elimination. It will be of importance to investigate the longevity of this transcriptomic footprint at the single-cell level, and to determine whether repeated reinfection cycles lead to its intensification. Importantly, these alterations in murine livers, which we show are similar to those of HCV-cured patients, are restricted to formerly LCMV-infected hepatocytes and differentiate them from virus-naive bystander cells. By extrapolation to the human setting, where cellular fate mapping of viral infection is impossible, these findings could mean that a substantial proportion of the transcriptomic alterations in actively or formerly HCV-infected livers is due to a hepatocyte-intrinsic imprint of viral infection, independent of immune cell-mediated inflammation or fibrosis. While LCMV has not been linked to carcinogenesis, it is tempting to speculate that the persistent transcriptome alterations imprinted by HCV, the oncogenesis of which remains ill-defined (Hoshida et al., 2013; Nakagawa et al., 2016), may be

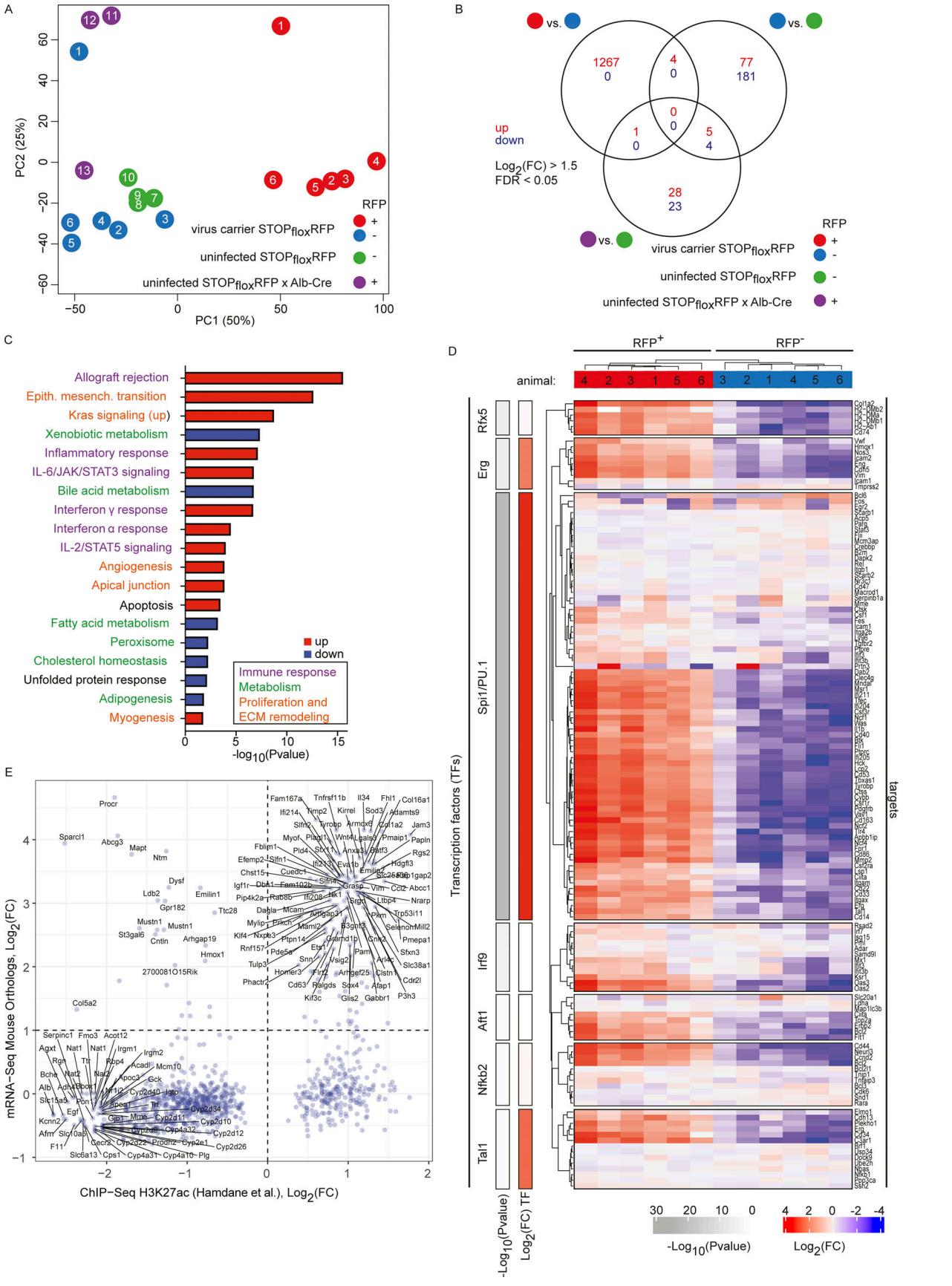

Figure 5. **Non-cytolytic clearance entails persistent transcriptome alterations. (A–D)** We infected neonatal STOP$_{flox}$RFP mice with artLCMV$_{Cre}$. 14 wk later, we isolated hepatocytes from RFP-positive (virus-cleared) and RFP-negative (uninfected) hepatocytes for RNA extraction and RNA sequencing. Control

hepatocytes were (RFP-negative) cells from uninfected $STOP_{flox}RFP$ mice and RFP-positive cells from $STOP_{flox}RFP$ × Alb-Cre mice. **(A)** Principal component analysis of FACS-sorted RFP-positive (virus-cleared, red) and RFP-negative (uninfected, blue) hepatocytes from $artLCMV_{Cre}$-infected mice (animals 1–6) and the indicated naive controls (animals 7–13). **(B)** The Venn diagram enumerates differentially expressed genes (Log_2[FC] > 1.5, FDR < 0.05) for the indicated comparisons. **(C)** Gene set enrichment analysis comparing RFP-positive (virus-cleared) versus RFP-negative hepatocytes (uninfected) from $artLCMV_{Cre}$-infected animals. The top enriched pathways (FDR < 0.05) from the MSigDb Hallmark Gene Sets are displayed. Color-coding assigns pathways to three superordinate terms: (1) immune response, (2) metabolism, and (3) proliferation and extracellular matrix (ECM) remodeling. **(D)** Gene set enrichment analysis of transcriptional networks (R package dorothea). We included enriched networks (FDR < 0.05) fulfilling the criteria (1) that the underlying TF was expressed in the hepatocytes analyzed and (2) that at least 20% of the TF's known target genes were up-regulated. Heatmaps visualize expression (Log_2[FC], blue/red color scheme) of the underlying TF and its target genes, respectively. P values of the enrichment ($-Log_{10}$[P value]) are indicated in grayscales. Independent validation of selected DEGs by qPCR is depicted in Fig. S4, A and B. **(E)** Scatter plot comparing H3K27ac changes observed by Hamdane et al. (2019) in DAA-cured HCV patients (group 2) to RNA levels of the respective mouse orthologs emerging from this study (A–D). Analogous comparisons to H3K27ac changes of a second cohort of DAA-cured patients and of actively HCV-infected patients are reported in Fig. S4, C and D, respectively. Key differentially expressed genes and TFs were independently validated by TaqMan RT-qPCR (Fig. S5, A and B). Epith. Mesench., epithelial–mesenchymal.

decisive for the consequences of exposure to other carcinogenic agents such as aflatoxin (Chu et al., 2018; Palliyaguru and Wu, 2013). The elevated incidence of hepatocellular carcinoma in HCV-cured individuals is compatible with this hypothesis (El-Serag et al., 2016; Hamdane et al., 2019).

For several decades, persistent LCMV infection of mice has served as a primary model to study viral clearance by adoptive cell therapy (Ahmed et al., 1987; Gegin and Lehmann-Grube, 1992; Lehmann-Grube et al., 1985; Oldstone et al., 1986; Planz et al., 1997; Tishon et al., 1993; Varho et al., 1981; Volkert, 1963). The present findings have obvious implications also on the interpretation of these earlier studies. The observation that transfer of immune spleen cells resulted in the rapid clearance of most organs including the liver but much delayed virus elimination from neurons (Oldstone et al., 1986) was, subsequently, interpreted to reflect differential level of T cell immunosurveillance owing to low levels of MHC class I on neurons (Joly et al., 1991; Tishon et al., 1993). While this interpretation remains viable in principle, the present findings open up the alternative possibility that cell-intrinsic elimination of LCMV from neurons takes longer than from hepatocytes, and that adoptive cell therapy merely prevented or slowed down the rate at which these cells were reinfected. The observation that effective elimination of persistent LCMV infection by adoptive spleen cell therapy required virus-specific B cells as a source of antiviral antibodies (Planz et al., 1997) supports this alternative hypothesis.

Another important concept, which studies in LCMV carriers have contributed to, consists of the noncytolytic, cytokine-mediated clearance of virus-infected hepatocytes (Guidotti et al., 1999a; Tishon et al., 1995). The present findings, albeit not providing any evidence to the contrary, demonstrate that virus clearance can also occur in a cell-intrinsic manner, independently of either type I IFN or type II IFN signaling. Future studies should investigate the relative contribution of cytokine-mediated virus clearance at the level of individual hepatocytes versus indirect effects on systemic viral loads, which are predicted to impact the reinfection rate of hepatocytes and thereby may also reduce the viral burden in the liver.

The molecular mechanisms underlying cell-intrinsic noncytolytic clearance of LCMV infection requires further investigation. The processes accountable in immortalized cell lines must obviously rely on either autonomous cell-intrinsic and autocrine mechanisms or potentially involves paracrine signaling, while immune cell effects are excluded. Among the candidate soluble factors that may contribute to clearance in mice, if any, lymphotoxins should be mentioned. They can be produced by several cell types (Ware, 2005) and have a prominent role in the pathogenesis of HCV-induced hepatocellular carcinoma (Browning and French, 2002; Haybaeck et al., 2009) as well as in the cell-intrinsic clearance of HBV (Lucifora et al., 2014). A potential contribution of innate lymphoid cells such as natural killer cells should also be investigated, albeit natural killer cells of AGRAG mice are immature and dysfunctional (Boyman et al., 2004) and thus are likely dispensable for noncytolytic LCMV clearance.

The present investigations on hepatocyte clearance in mice relied entirely on the neonatal infection model. Antiviral T cell tolerance, one of its immunological hallmarks (Pircher et al., 1989), but possibly also the use of a transgenic and therefore attenuated reporter virus (Kallert et al., 2017), may have impacted the relative contribution of noncytolytic and cytolytic clearance mechanisms to virus control in tissues. Of note, however, congenital infection by vertical transmission represents the natural habitat of LCMV in the wild. Accordingly, LCMV has evolved to persist in a T cell–tolerant host, and the viruses' susceptibility to cell-intrinsic clearance mechanisms may help assuring virus–host balance and long-term healthy coexistence. It seems plausible that a similar pathogen–host relationship predominates when HCV infection progresses to chronicity and antiviral T cells get functionally exhausted (Thimme, 2021).

We provide evidence that the well-known wave-like infection dynamics of LCMV-infected cell cultures (Hotchin, 1973a; Hotchin, 1973b; Hotchin, 1974; King et al., 2018; Weber et al., 1983) are due, at least in part, to noncytolytic clearance and superinfection exclusion. Using Z protein–deficient LCMV (Zaza et al., 2018), we find that the Z protein, albeit a negative regulator of viral transcription and genome replication (Cornu and de la Torre, 2001; Kranzusch and Whelan, 2011), is dispensable for superinfection exclusion of arenavirus-infected cells. It therefore seems unlikely that Z protein in its putative role as a viral molecular clock (Kranzusch and Whelan, 2011) extinguishes LCMV infection in cells. This postulate assumes, however, that cell-intrinsic noncytolytic clearance of LCMV and superinfection exclusion reflect two manifestations of the same underlying molecular events. While we consider this to be highly likely, we acknowledge that this assumption remains uncertain in the absence of a detailed molecular understanding.

Unraveling the mechanisms that underlie cell-intrinsic noncytolytic elimination of persistent RNA virus infection may reveal an Achilles' heel of these infections. The demonstration herein of cell-intrinsic noncytolytic RNA virus clearance, therefore, furthers our understanding of complications arising from such infection while simultaneously opening up new avenues for their treatment.

Materials and methods

Cell lines

BHK-21 cells were obtained from the European Collection of Authenticated Cell Cultures (clone 13; 85011433) and cultured in DMEM (Sigma-Aldrich) complemented with 10% FCS, 1 M Hepes, 100 mM sodium pyruvate, and 1× Tryptose Phosphate Broth (50× mix; Gibco). BHK-21 cells expressing the LCMV GP and the LCMV NP respectively, have been described previously (Darbre et al., 2015; Flatz et al., 2010) and were cultured in the presence of 2 µg/ml puromycin. LCMV GP expressing HEK293T cells (293T-GP) were described previously (Flatz et al., 2010) and were cultured in DMEM containing 10% FCS and 2 µg/ml puromycin. NIH/3T3 cells were obtained from the American Type Culture Collection (CRL-1658) and cultured in DMEM containing 10% FCS. $A549_{floxGFP}$ and $Vero_{floxGFP}$ cells were kindly provided by Martin Schwemmle, University of Freiburg, Freiburg, Germany. These cells were generated by retroviral transduction as described (Reuther et al., 2015) using the pMSCV-loxp-dsRed-loxp-eGFP-Puro-WPRE plasmid (Addgene plasmid 32702; donated by Hans Clevers, Hubrecht institute, Utrecht, Netherlands) and were cultured in the same medium as 293T-GP cells. For long-term culture of $A549_{floxGFP}$ and $Vero_{floxGFP}$ cells, cells were split three times a week at a 1:3 ratio.

Isolation and culture of primary murine hepatocytes

Animals were euthanized with CO_2 followed by immediate perfusion of the liver via the inferior vena cava with 20 ml HBSS (GIBCO) supplemented with 0.5 mM EGTA (Sigma-Aldrich). The liver was digested with 20 ml prewarmed (40°C) digestion medium (L15 medium [GIBCO] containing 40 mg/l Liberase [Roche]) using a peristaltic pump (5 ml/min). Subsequent to the isolation of the organ, the liver capsule was dissected in a Petri dish containing 10 ml digestion medium. Hepatocytes were passed through a 70-µm cell strainer and centrifuged (50 *g* for 10 min at 4°C) and washed twice with 30 ml William's E medium (GIBCO) containing 1% penicillin-streptomycin and 10% FCS. For ex vivo infection, cells were plated in 6-well plates (0.8 × 10e6 cells/well) coated with rat tail collagen I (Corning). 3 h after plating, cells were washed twice with PBS and the medium was exchanged for William's E medium containing 1% penicillin-streptomycin and 0.5% FCS. For long-term culture, medium was exchanged three times a week.

Viruses, virus generation, and virus titration

The genetic engineering and rescue from cDNA of artLCMV, LCMVΔGP, and LCMVΔNP viruses and vectors were performed as described (Darbre et al., 2015; Flatz et al., 2006; Flatz et al., 2010; Kallert et al., 2017). The artLCMV and LCMVΔGP viruses used in this study are based on the Armstrong Clone 13 (Cl13) backbone (Flatz et al., 2006), but encode (artLCMV) or are pseudotyped with the GP of the LCMV strain WE. Sequences encoding Cre, GFP, dTomato, and Thy1.1 were PCR-amplified from plasmids containing the respective open reading frames. To generate LCMV encoding an N-terminally Flag(DYKDDDDK)-tagged NP, a primer comprising the Flag-tag sequence was used to amplify the NP gene. For the generation of $LCMV\Delta Z_{Cre}$, the Z-encoding sequence of the pI-L-Cl13(–) plasmid (Flatz et al., 2006) was exchanged for a synthetic, Cre-encoding sequence resulting in pI-L_Cre_IGR_L (Genscript). For the rescue of Z-deficient viruses, 0.1 µg of a Z-encoding pCAGGs expression plasmid (pC-Z) was added to the rescue mix as described (Zaza et al., 2018). 6 d after transfection of BHK-21 cells with pI-L_Cre_IGR_L and combination with the other LCMV rescue plasmids, cells were co-cultured with puromycin-resistant $A549_{floxGFP}$ cells at a 1:1 ratio representing the start of the experiment depicted in Fig. 4 A. 3 d later, BHK-21 cells were eliminated from the co-culture by the addition of 2 µg/ml puromycin to the medium.

Virus stock and blood titers of artLCMV and LCMVΔGP were determined by immunofocus assay on NIH/3T3 cells and 293T-GP cells, respectively, using a rat-anti-LCMV NP antibody (VL-4) for detection of virus-infected cells as described (Battegay et al., 1991). NP-deficient viruses were quantified on BHK-21 cells expressing the LCMV NP using a mouse anti–LCMV GP antibody (83.4; Eschli et al., 2007) as reported previously (Darbre et al., 2015). $STOP_{flox}$-RFP mice and $STOP_{flox}$-RFP–derived hepatocytes were infected with an artLCMV encoding Cre in cis with the viral NP on the first S segment and a GFP together with the viral GP on the second S segment. For infection of $STOP_{flox}$-eYFP mice, $A549_{floxGFP}$ cells, and $Vero_{floxGFP}$ cells, an artLCMV encoding a red fluorescent tomato protein on the second, GP-encoding S segment was used. For infection of R26R-Confetti mice, we used a virus encoding a Cre transgene on both S segments.

Flow cytometry and FACS

Live/dead staining was performed with the Zombie UV Fixable viability kit (BioLegend, used for hepatocytes) or the Zombie Yellow Fixable viability kit (BioLegend, used for $A549_{floxGFP}$ cells in Fig. S4 G). To determine the proliferation rate of $A549_{floxGFP}$ cells in Fig. S4 F, cells were stained with the CellTrace Violet Cell Proliferation Kit (Thermo Fisher Scientific). Antibodies against Thy1.1 (Ox-7, BV421-conjugated; BioLegend) and the Flag-tag (L5, APC-conjugated; BioLegend) were used at a 1:100 dilution. The rat-anti-LCMV NP antibody (VL-4, hybridoma supernatant) was conjugated to Alexa Fluor 647 using the Alexa Fluor 647 Antibody Labeling Kit (Invitrogen) and was diluted 1:1,000. Cells were stained for 30 min at 4°C. For intracellular staining, cells were fixed for 15 min at room temperature (PBS/2% paraformaldehyde [PFA]) and permeabilized for 5 min in permeabilization buffer (FACS buffer/0.1% saponin). Labeled cells were measured on an LSRFortessa (Becton Dickinson) flow cytometer. For the isolation of nucleic acids, cells were sorted on a FACSAria III (Becton Dickinson).

Immunohistochemistry and immunofluorescence

Liver tissue was fixed in 4% PFA and embedded in paraffin. Subsequent to inactivation of endogenous peroxidases with PBS/3% hydrogen peroxide, tissue sections were blocked with PBS/10% FCS. For immunohistochemical staining of LCMV NP and eYFP, samples were incubated overnight (4°C) with rabbit-anti LCMV NP serum (diluted 1:10,000) and rabbit anti-GFP antibody (diluted 1:200; D5.1; Cell Signaling), respectively. Bound primary antibodies were incubated with the ImmPRESS HRP Goat Anti-Rabbit IgG Polymer Detection Kit (Vector Laboratories) for 30 min before treatment with 3,3′-diaminobenzidine (Dako). For immunofluorescent staining of eYFP, sections were treated as described above, and bound HRP was visualized with the TSA plus Cyanin 3 kit (Perkin Elmer). For fluorescent costaining of LCMV-NP, sections were treated with Fab mouse IgG Block (Jackson ImmunoResearch) and incubated with rat anti–LCMV NP serum (diluted 1:1,000) for 1 h at room temperature. Bound primary antibody was stained with Alexa Fluor 647–labeled donkey anti-rat antibody (diluted 1:200; AB_2340694; Jackson ImmunoResearch). Immunofluorescent staining of RFP was performed with a rabbit anti-RFP antibody (diluted 1:400; ab124754; Abcam) followed by incubation with a HRP goat anti-rabbit IgG polymer (K4003; Dako). Bound HRP was visualized with the Opal 570 reagent (Akoya Biosciences). For fluorescent costaining of GFP derivates, sections were incubated with a chicken anti-GFP antibody (diluted 1:200; CGFP-45ALY-Z; ICL). Bound GFP antibody was visualized with an A647-labeled goat anti-chicken antibody (diluted 1:200; A21449; Life). Hemalum (Merck) and DAPI (Invitrogen) were used to counterstain nuclei in brightfield and fluorescence microscopy, respectively. Immunohistochemical staining for RFP was performed with the Ventana Discovery Ultra (Roche Diagnostics [Suisse] SA) automated slide stainer. In brief, tissue sections were deparaffinized and rehydrated. Antigen was retrieved by heat in Cell Conditioning buffer 1 (CC1; 950–124; Ventana) at 95°C for 40 min. Primary antibody (preadsorbed anti-RFP; 600–401-379; 1:100 dilution; Rockland Antibodies and Assays) was manually applied and incubated for 1 h at 37°C. After washing, the HRP-polymer secondary antibody (anti-rabbit polymer HRP; 414141F; Nichirei Histofine Simple Stain MAX PO) was incubated for 1 h at 37°C. Detection was performed with the Ventana DISCOVERY ChromoMap DAB (760–159; Ventana) detection kit. Afterward, the slides were counterstained with hematoxylin II, followed by bluing reagent (respectively, 790–2208 and 760–2037; Ventana). Sections were then dehydrated, cleared, and mounted with permanent mounting. Slides stained for LCMV NP, GFP, and RFP (fluorescent) were scanned using a MIRAX Midi slide scanner (ZEISS) or a Panoramic Flash (3D Histech) at 200× magnification. Slides stained immunohistochemically for RFP were scanned with the Hamamatsu NanoZoomer S60.

RNA in situ hybridization

Detection of viral RNA by in situ hybridization was performed on liver sections fixed in 4% PFA using the ViewRNA ISH Tissue Assay (Thermo Fisher Scientific) as previously described (Calabrese and Wieland, 2017) with the following changes in the protocol: probe-set dilution, 1:30; hybridization time, 2.5 h; preamplification and amplification time, 40 min; and label probe-AP dilution, 1:500. For specific detection of NP coding, LCMV S-segment RNA, we used a custom-made type I probe set (Thermo Fisher Scientific) binding to the negatively oriented LCMV NP gene (GenBank: KY514256.1; nucleotides 1640..3316). Stained slides were acquired in brightfield and in fluorescence (tetramethylrhodamine-isothiocyanate filter) using a slide scanner Hamamatsu NanoZoomer S60. The raw image files were converted in 8-bit grayscale files and overlaid to obtain the merged composite images using ImageJ.

RNA isolation and RT-qPCR

For total cellular RNA isolation from organs and cultured cells, samples were collected in TRI Reagent (Sigma-Aldrich). Organ samples were subsequently homogenized using the TissueLyser II (Qiagen). For bulk analysis of isolated hepatocytes, cells were sorted directly into TRI Reagent LS (Sigma-Aldrich). RNA was extracted using the Direct-zol RNA MicroPrep kit (Zymo Research). NP-coding, LCMV RNA was quantified as previously described (Pinschewer et al., 2010). Applied Biosystems TaqMan kits (Thermo Fisher Scientific) were used to determine mRNA levels of PDGFRα (Mm00440701_m1), PDGFRβ (Mm00435546_m1), PDGFβ (Mm00440677_m1), Col1a1 (Mm00801666_g1), Col1a2 (Mm00483888_m1), Col4a1 (Mm01210125_m1), Loxl2 (Mm00804740_m1), H2-Ab1 (Mn00439216_m1), HGF (Mm01135184_m1), TLR4 (Mm00445273_m13), OAS3 (Mm00460944_m1), TGFβ1 (Mm01178820_m1), CTGF (Mm01192933_g1), GAPDH (NM_008084.2), Spi1 (Mm00488140_m1), Erg (Mm01214244_m1), and Tal1 (Mm01187033_m1). RT-qPCR was performed with Superscript III One Step Platinum Taq (Thermo Fisher Scientific). Samples with cycle threshold (Ct) values >40 were considered negative. For quantitative single-cell RT-qPCR, we used the CellsDirect One-Step qRT-PCR Kit (Thermo Fisher Scientific). Single hepatocytes were sorted into 5 µl of lysis solution. After lysis, we added 5 µl of diethyl pyrocarbonate–treated, nuclease-free water (Thermo Fisher Scientific). Levels of NP-encoding LCMV RNA were determined from nine tenths of the lysate. Expression levels were normalized to that of GAPDH, which we measured in the remaining one tenth of the sample. Samples with Ct_{GAPDH} >40 were excluded, and samples with Ct_{NP} >35 were considered negative.

Next-generation sequencing and data analysis

mRNA-Seq libraries were prepared from RNA isolated from 50,000 sorted hepatocytes using the TruSeq kit (Illumina). For sequencing, an Illumina NextSeq 500 was used performing two 38-bp paired-end runs. Reads were aligned to the mouse mm10 genome using STAR (version 2.7.0c) and setting options for multi-mapping reads to "–outFilterMultimapNmax 10–outSAMmultNmax 1" (Dobin et al., 2013). Gene expression was quantified with featureCounts (Subread version 1.6.4) and extra options "-O–read2pos 5 –M –s 2 –p -B" and relied on gene annotation from Ensemble (version 94; Liao et al., 2014). All further analysis was performed within the R/Bioconductor framework (R version 3.5.0/Bioconductor version 3.8). Genes

were filtered for a log-counts per million reads>0 in at least two samples (n = 12,251 genes). Differential expression analysis was performed with the Bioconductor package edgeR and using two different designs (McCarthy et al., 2012). A within-subject design was chosen to contrast RFP$^+$ versus RFP$^-$ cells in infected animals. A second design compared RFP$^+$ cells from infected and naive animals, as well as RFP$^+$ versus RFP$^-$ cells from naive animals. This between-subjects design also accounted for the sex of the animals. The edgeR functions glmQLFit and glmQLFTest were used to calculate log-fold-changes and false discovery rate (FDR)–adjusted P values for all contrasts of interest. A function camera from the edgeR package was used to evaluate differential regulation of gene sets from MSigDb (version 6.0). The ComplexHeatmap package was used to draw heatmaps (Gu et al., 2016). The TF target gene resource for mouse from the R package dorothea was used to evaluate differential TF activity across RFP$^+$ versus RFP$^-$ cells in infected animals (Garcia-Alonso et al., 2019). Here, the camera function from edgeR was used to test TF target gene sets with at least 10 members and confidence levels A and B for differential regulation. The evaluation only included expressed TFs, according to the above criteria. Comparison to altered gene expression in the context of HCV liver infection relied on a supplementary gene list published by Hamdane et al. (2019). The list was translated to mouse orthologs, to the extent they are defined, using ensemble biomart and subsetted to the expressed genes in our study. This gave rise to 1,015 (HCV infection and DAA cure in patients: 2,193 genes) expressed mouse orthologs for which logFCs could be directly compared. The raw mRNA-Seq datasets of Boldanova et al. (2017) (accession no. GSE84346; HCV-infected + control samples) and Hamdane et al. (2019) (DAA-cured and control) were downloaded from GEO and mapped with STAR (version 2.7.0c) to the human hg38 analysis set genome. Genes were quantified with featureCounts (Subread version 1.6.4), and differential expression analysis was performed with the Bioconductor package edgeR. Ensembl biomart was used to map human genes to mouse orthologs. Mouse orthologs that were up-regulated with a logFC >1 were tested for enrichment among the mouse RFP$^+$ versus RFP$^-$ regulated genes using the cameraPR function of the limma package.

Animal experimentation

STOP$_{flox}$-RFP mice (B6.CG-GT[ROSA]26Sortm1Hjf; on C57BL/6 background; Luche et al., 2007), STOP$_{flox}$-eYFP mice (B6.129X1-Gt[ROSA]26Sortm1[EYFP]Cos/J, backcrossed to C57BL/6 and >98% pure by single nucleotide polymorphism typing; Srinivas et al., 2001) and R26R-Confetti mice (Gt[ROSA]26Sortm1[CAG-Brainbow2.1]Cle/J; backcrossed to C57BL/6 for at least three generations; Livet et al., 2007) have been described. RAG-1 × STOP$_{fl}$-RFP mice were generated by crossing STOP$_{flox}$-RFP mice to B6.RAG-1 mice (Rag-1$^{-/-}$; backcrossed to C57BL/6 for at least 10 generations and 99% genetically pure by single nucleotide polymorphism typing; Mombaerts et al., 1992). AGRAG × STOP$_{flox}$-RFP mice resulted from crossing RAG1 × STOP$_{flox}$-RFP mice to B6.AGRAG mice (type I IFN receptor$^{-/-}$, type II IFN receptor$^{-/-}$, Rag-1$^{-/-}$, each founding line backcrossed to C57BL/6 for at least 10 generations or generated on C57BL/6 background, respectively; Grob et al., 1999). For neonatal infection, male and female mice were injected intracranially within 24 h after birth with a total volume of 25 µl containing 2.5×10^4 focus forming units of the respective virus. Uninfected litters were used as noncarrier controls. For adult infection, male and female mice were infected i.v. with 7×10^5 focus forming units of artLCMV$_{Cre}$. Animal experiments were performed at the University of Basel in accordance with the Swiss law for animal protection and with permission by the Veterinäramt Basel-Stadt.

Quantification and statistical analysis

Error bars represent mean ± SEM or mean ± SD as reported in the figure legends. To compare two groups, two-tailed Student's t test was used as indicated in the figure legends (unpaired or paired). Two-way ANOVA with Bonferroni's post-test was used for multiple comparisons. Statistical significance is indicated in the figures as ‡, P < 0.1; *, P < 0.05; **, P < 0.01; GraphPad Prism8 was used for statistical analysis.

Online supplemental material

Fig. S1 reports the evaluation of artLCMVCre as a tool to induce Cre recombination exclusively in cells replicating the viral genome, the analysis of LCMV-infected mouse hepatocytes in vivo and in cell culture, and the occurrence of cleared cells in lung, kidney, and ileum. Fig. S2 displays the analysis of viral replication in mice infected neonatally or at adult age with artLCMVCre. Fig. S3 shows the clonality fate mapping of virus-cleared mouse hepatocytes in vivo and the visualization of noncytolytically cleared hepatocytes of RAG-1–deficient mice. Fig. S4 depicts the gating strategy to detect GFP, Thy1.1, and NP-Flag–expressing cells as well as the characterization of cultured cells cleared from infection. Fig. S5 provides a validation of differentially expressed genes and comparison of LCMV transcriptomic footprint to HCV-cured and -infected patients. Table S1 shows a comparison of H3K27ac changes observed in HCV-infected or DAA-cured patients with changes of mRNA levels between RFP-positive and RFP-negative hepatocytes of mice neonatally infected with artLCMV$_{Cre}$.

Data availability

The data reported in this study are deposited in Zenodo open data repository (CERN), available at https://doi.org/10.5281/zenodo.5119267. Oligonucleotide primer sequences are available from the authors upon request. RNA sequencing data are deposited in GEO (accession no. GSE157431).

Acknowledgments

We thank Martin Schwemmle (University of Freiburg, Freiburg, Germany) for providing reagents and valuable comments on the manuscript. We are grateful to Stefan Wieland and Matthias Matter for helpful discussion. We are grateful to Karsten Stauffer for outstanding animal handling and care, as well as to Ingrid Wagner, Karim Hammad, and Cynthia Saadi for excellent tissue processing and histology.

This work was supported by the Swiss National Science Foundation (grant no. 310030_173132 to D.D. Pinschewer). D.

Merkler is supported by the Swiss National Science Foundation (grant nos. 310030B_201271 and 310030_185321) and the European Research Council (grant no. 865026).

Author contributions: P. Reuther, K. Martin, D. Merkler, and D.D. Pinschewer contributed to experimental conception and design. P. Reuther, K. Martin, M. Ciancaglini, and D. Calabrese performed experiments. P. Reuther, K. Martin, D. Calabrese, M. Kreutzfeldt, F. Geier, and D. Merkler analyzed and/or interpreted the data. D.D. Pinschewer and P. Reuther wrote the manuscript.

Disclosures: D.D. Pinschewer reported grants, personal fees, non-financial support, and "other" from Hookipa Pharma Inc. outside the submitted work; in addition, D.D. Pinschewer had a patent to PCT/EP14/055144 issued "Hookipa Pharma Inc.," a patent to PCT/EP14/055144 licensed "Hookipa Pharma Inc.," a patent to PCT/EP14/055144 with royalties paid "Hookipa Pharma Inc.," a patent to PCT/EP2015/076458 issued "Hookipa Pharma Inc.," a patent to PCT/EP2015/076458 licensed "Hookipa Pharma Inc.," a patent to PCT/EP2015/076458 with royalties paid "Hookipa Pharma Inc.," a patent to PCT/EP/08/010994 issued "Hookipa Pharma Inc.," a patent to PCT/EP/08/010994 licensed "Hookipa Pharma Inc.," a patent to PCT/EP/08/010994 with royalties paid "Hookipa Pharma Inc.," a patent to PCT/EP2017/061865 issued "Hookipa Pharma Inc.," a patent to PCT/EP2017/061865 licensed "Hookipa Pharma Inc.," and a patent to PCT/EP2017/061865 with royalties paid. D.D. Pinschewer is a founder, consultant, and shareholder of Hookipa Pharma Inc. and holds stock options of Hookipa Pharma Inc. commercializing arenavirus-based vector technology. No other disclosures were reported.

Submitted: 18 February 2021
Revised: 14 June 2021
Accepted: 28 July 2021

References

Ahmed, R., B.D. Jamieson, and D.D. Porter. 1987. Immune therapy of a persistent and disseminated viral infection. *J. Virol.* 61:3920–3929. https://doi.org/10.1128/jvi.61.12.3920-3929.1987

Allweiss, L., T. Volz, K. Giersch, J. Kah, G. Raffa, J. Petersen, A.W. Lohse, C. Beninati, T. Pollicino, S. Urban, et al. 2018. Proliferation of primary human hepatocytes and prevention of hepatitis B virus reinfection efficiently deplete nuclear cccDNA in vivo. *Gut.* 67:542–552. https://doi.org/10.1136/gutjnl-2016-312162

Battegay, M., S. Cooper, A. Althage, J. Bänziger, H. Hengartner, and R.M. Zinkernagel. 1991. Quantification of lymphocytic choriomeningitis virus with an immunological focus assay in 24- or 96-well plates. *J. Virol. Methods.* 33:191–198. https://doi.org/10.1016/0166-0934(91)90018-U

Bergthaler, A., D. Merkler, E. Horvath, L. Bestmann, and D.D. Pinschewer. 2007. Contributions of the lymphocytic choriomeningitis virus glycoprotein and polymerase to strain-specific differences in murine liver pathogenicity. *J. Gen. Virol.* 88:592–603. https://doi.org/10.1099/vir.0.82428-0

Bergthaler, A., L. Flatz, A. Verschoor, A.N. Hegazy, M. Holdener, K. Fink, B. Eschli, D. Merkler, R. Sommerstein, E. Horvath, et al. 2009. Impaired antibody response causes persistence of prototypic T cell-contained virus. *PLoS Biol.* 7:e1000080. https://doi.org/10.1371/journal.pbio.1000080

Binder, G.K., and D.E. Griffin. 2001. Interferon-γ-mediated site-specific clearance of alphavirus from CNS neurons. *Science.* 293:303–306. https://doi.org/10.1126/science.1059742

Bogomolov, P., A. Alexandrov, N. Voronkova, M. Macievich, K. Kokina, M. Petrachenkova, T. Lehr, F.A. Lempp, H. Wedemeyer, M. Haag, et al. 2016. Treatment of chronic hepatitis D with the entry inhibitor myrcludex B: First results of a phase Ib/IIa study. *J. Hepatol.* 65:490–498. https://doi.org/10.1016/j.jhep.2016.04.016

Boldanova, T., A. Suslov, M.H. Heim, and A. Necsulea. 2017. Transcriptional response to hepatitis C virus infection and interferon-alpha treatment in the human liver. *EMBO Mol. Med.* 9:816–834. https://doi.org/10.15252/emmm.201607006

Boyman, O., H.P. Hefti, C. Conrad, B.J. Nickoloff, M. Suter, and F.O. Nestle. 2004. Spontaneous development of psoriasis in a new animal model shows an essential role for resident T cells and tumor necrosis factor-alpha. *J. Exp. Med.* 199:731–736. https://doi.org/10.1084/jem.20031482

Browning, J.L., and L.E. French. 2002. Visualization of lymphotoxin-β and lymphotoxin-β receptor expression in mouse embryos. *J. Immunol.* 168:5079–5087. https://doi.org/10.4049/jimmunol.168.10.5079

Burdeinick-Kerr, R., and D.E. Griffin. 2005. Gamma interferon-dependent, noncytolytic clearance of sindbis virus infection from neurons in vitro. *J. Virol.* 79:5374–5385. https://doi.org/10.1128/JVI.79.9.5374-5385.2005

Burdeinick-Kerr, R., D. Govindarajan, and D.E. Griffin. 2009. Noncytolytic clearance of sindbis virus infection from neurons by gamma interferon is dependent on Jak/STAT signaling. *J. Virol.* 83:3429–3435. https://doi.org/10.1128/JVI.02381-08

Calabrese, D., and S.F. Wieland. 2017. Highly Sensitive Detection of HBV RNA in Liver Tissue by In Situ Hybridization. *Methods Mol. Biol.* 1540:119–134. https://doi.org/10.1007/978-1-4939-6700-1_10

Chambers, B.S., B.E. Heaton, K. Rausch, R.E. Dumm, J.R. Hamilton, S. Cherry, and N.S. Heaton. 2019. DNA mismatch repair is required for the host innate response and controls cellular fate after influenza virus infection. *Nat. Microbiol.* 4:1964–1977. https://doi.org/10.1038/s41564-019-0509-3

Chu, Y.-J., H.-I. Yang, H.-C. Wu, M.-H. Lee, J. Liu, L.-Y. Wang, S.-N. Lu, C.-L. Jen, S.-L. You, R.M. Santella, and C.-J. Chen. 2018. Aflatoxin B_1 exposure increases the risk of hepatocellular carcinoma associated with hepatitis C virus infection or alcohol consumption. *Eur. J. Cancer.* 94:37–46. https://doi.org/10.1016/j.ejca.2018.02.010

Clayton, D.F., and J.E. Darnell Jr. 1983. Changes in liver-specific compared to common gene transcription during primary culture of mouse hepatocytes. *Mol. Cell. Biol.* 3:1552–1561. https://doi.org/10.1128/MCB.3.9.1552

Cole, G.A., N. Nathanson, and R.A. Prendergast. 1972. Requirement for theta-bearing cells in lymphocytic choriomeningitis virus-induced central nervous system disease. *Nature.* 238:335–337. https://doi.org/10.1038/238335a0

Cornu, T.I., and J.C. de la Torre. 2001. RING finger Z protein of lymphocytic choriomeningitis virus (LCMV) inhibits transcription and RNA replication of an LCMV S-segment minigenome. *J. Virol.* 75:9415–9426. https://doi.org/10.1128/JVI.75.19.9415-9426.2001

Cornu, T.I., H. Feldmann, and J.C. de la Torre. 2004. Cells expressing the RING finger Z protein are resistant to arenavirus infection. *J. Virol.* 78:2979–2983. https://doi.org/10.1128/JVI.78.6.2979-2983.2004

Damonte, E.B., S.E. Mersich, and C.E. Coto. 1983. Response of cells persistently infected with arenaviruses to superinfection with homotypic and heterotypic viruses. *Virology.* 129:474–478. https://doi.org/10.1016/0042-6822(83)90185-X

Darbre, S., S. Johnson, S. Kallert, P.H. Lambert, C.A. Siegrist, and D.D. Pinschewer. 2015. The Nucleoprotein Is Required for Lymphocytic Choriomeningitis Virus-Based Vaccine Vector Immunogenicity. *J. Virol.* 89:11734–11738. https://doi.org/10.1128/JVI.01613-15

de Jong, Y.P., M. Dorner, M.C. Mommersteeg, J.W. Xiao, A.B. Balazs, J.B. Robbins, B.Y. Winer, S. Gerges, K. Vega, R.N. Labitt, et al. 2014. Broadly neutralizing antibodies abrogate established hepatitis C virus infection. *Sci. Transl. Med.* 6:254ra129. https://doi.org/10.1126/scitranslmed.3009512

Desmyter, J., J.L. Melnick, and W.E. Rawls. 1968. Defectiveness of interferon production and of rubella virus interference in a line of African green monkey kidney cells (Vero). *J. Virol.* 2:955–961. https://doi.org/10.1128/jvi.2.10.955-961.1968

Dobin, A., C.A. Davis, F. Schlesinger, J. Drenkow, C. Zaleski, S. Jha, P. Batut, M. Chaisson, and T.R. Gingeras. 2013. STAR: ultrafast universal RNA-seq aligner. *Bioinformatics.* 29:15–21. https://doi.org/10.1093/bioinformatics/bts635

Dufton, N.P., C.R. Peghaire, L. Osuna-Almagro, C. Raimondi, V. Kalna, A. Chauhan, G. Webb, Y. Yang, G.M. Birdsey, P. Lalor, et al. 2017. Dynamic regulation of canonical TGFβ signalling by endothelial transcription factor ERG protects from liver fibrogenesis. *Nat. Commun.* 8:895. https://doi.org/10.1038/s41467-017-01169-0

Dumm, R.E., J.K. Fiege, B.M. Waring, C.T. Kuo, R.A. Langlois, and N.S. Heaton. 2019. Non-lytic clearance of influenza B virus from infected cells preserves epithelial barrier function. *Nat. Commun.* 10:779. https://doi.org/10.1038/s41467-019-08617-z

El-Serag, H.B., F. Kanwal, P. Richardson, and J. Kramer. 2016. Risk of hepatocellular carcinoma after sustained virological response in Veterans with hepatitis C virus infection. *Hepatology.* 64:130–137. https://doi.org/10.1002/hep.28535

Ellenberg, P., M. Edreira, and L. Scolaro. 2004. Resistance to superinfection of Vero cells persistently infected with Junin virus. *Arch. Virol.* 149: 507–522. https://doi.org/10.1007/s00705-003-0227-1

Eschli, B., R.M. Zellweger, A. Wepf, K.S. Lang, K. Quirin, J. Weber, R.M. Zinkernagel, and H. Hengartner. 2007. Early antibodies specific for the neutralizing epitope on the receptor binding subunit of the lymphocytic choriomeningitis virus glycoprotein fail to neutralize the virus. *J. Virol.* 81:11650–11657. https://doi.org/10.1128/JVI.00955-07

Flatz, L., A. Bergthaler, J.C. de la Torre, and D.D. Pinschewer. 2006. Recovery of an arenavirus entirely from RNA polymerase I/II-driven cDNA. *Proc. Natl. Acad. Sci. USA.* 103:4663–4668. https://doi.org/10.1073/pnas.0600652103

Flatz, L., A.N. Hegazy, A. Bergthaler, A. Verschoor, C. Claus, M. Fernandez, L. Gattinoni, S. Johnson, F. Kreppel, S. Kochanek, et al. 2010. Development of replication-defective lymphocytic choriomeningitis virus vectors for the induction of potent CD8+ T cell immunity. *Nat. Med.* 16:339–345. https://doi.org/10.1038/nm.2104

Fung-Leung, W.P., T.M. Kündig, R.M. Zinkernagel, and T.W. Mak. 1991. Immune response against lymphocytic choriomeningitis virus infection in mice without CD8 expression. *J. Exp. Med.* 174:1425–1429. https://doi.org/10.1084/jem.174.6.1425

Garcia-Alonso, L., C.H. Holland, M.M. Ibrahim, D. Turei, and J. Saez-Rodriguez. 2019. Benchmark and integration of resources for the estimation of human transcription factor activities. *Genome Res.* 29: 1363–1375. https://doi.org/10.1101/gr.240663.118

Gegin, C., and F. Lehmann-Grube. 1992. Control of acute infection with lymphocytic choriomeningitis virus in mice that cannot present an immunodominant viral cytotoxic T lymphocyte epitope. *J. Immunol.* 149: 3331–3338.

Griffin, D.E. 2010. Recovery from viral encephalomyelitis: immune-mediated noncytolytic virus clearance from neurons. *Immunol. Res.* 47:123–133. https://doi.org/10.1007/s12026-009-8143-4

Grob, P., V.E.C.J. Schijns, M.F. van den Broek, S.P.J. Cox, M. Ackermann, and M. Suter. 1999. Role of the individual interferon systems and specific immunity in mice in controlling systemic dissemination of attenuated pseudorabies virus infection. *J. Virol.* 73:4748–4754. https://doi.org/10.1128/JVI.73.6.4748-4754.1999

Gu, Z., R. Eils, and M. Schlesner. 2016. Complex heatmaps reveal patterns and correlations in multidimensional genomic data. *Bioinformatics.* 32: 2847–2849. https://doi.org/10.1093/bioinformatics/btw313

Guidotti, L.G., and F.V. Chisari. 2001. Noncytolytic control of viral infections by the innate and adaptive immune response. *Annu. Rev. Immunol.* 19: 65–91. https://doi.org/10.1146/annurev.immunol.19.1.65

Guidotti, L.G., K. Ando, M.V. Hobbs, T. Ishikawa, L. Runkel, R.D. Schreiber, and F.V. Chisari. 1994. Cytotoxic T lymphocytes inhibit hepatitis B virus gene expression by a noncytolytic mechanism in transgenic mice. *Proc. Natl. Acad. Sci. USA.* 91:3764–3768. https://doi.org/10.1073/pnas.91.9.3764

Guidotti, L.G., P. Borrow, M.V. Hobbs, B. Matzke, I. Gresser, M.B. Oldstone, and F.V. Chisari. 1996a. Viral cross talk: intracellular inactivation of the hepatitis B virus during an unrelated viral infection of the liver. *Proc. Natl. Acad. Sci. USA.* 93:4589–4594. https://doi.org/10.1073/pnas.93.10.4589

Guidotti, L.G., T. Ishikawa, M.V. Hobbs, B. Matzke, R. Schreiber, and F.V. Chisari. 1996b. Intracellular inactivation of the hepatitis B virus by cytotoxic T lymphocytes. *Immunity.* 4:25–36. https://doi.org/10.1016/S1074-7613(00)80295-2

Guidotti, L.G., P. Borrow, A. Brown, H. McClary, R. Koch, and F.V. Chisari. 1999a. Noncytopathic clearance of lymphocytic choriomeningitis virus from the hepatocyte. *J. Exp. Med.* 189:1555–1564. https://doi.org/10.1084/jem.189.10.1555

Guidotti, L.G., R. Rochford, J. Chung, M. Shapiro, R. Purcell, and F.V. Chisari. 1999b. Viral clearance without destruction of infected cells during acute HBV infection. *Science.* 284:825–829. https://doi.org/10.1126/science.284.5415.825

Hamdane, N., F. Jühling, E. Crouchet, H. El Saghire, C. Thumann, M.A. Oudot, S. Bandiera, A. Saviano, C. Ponsolles, A.A. Roca Suarez, et al. 2019. HCV-Induced Epigenetic Changes Associated With Liver Cancer Risk Persist After Sustained Virologic Response. *Gastroenterology.* 156:2313–2329.e7. https://doi.org/10.1053/j.gastro.2019.02.038

Hamilton, J.R., D. Sachs, J.K. Lim, R.A. Langlois, P. Palese, and N.S. Heaton. 2016. Club cells surviving influenza A virus infection induce temporary nonspecific antiviral immunity. *Proc. Natl. Acad. Sci. USA.* 113: 3861–3866. https://doi.org/10.1073/pnas.1522376113

Hausmann, J., A. Pagenstecher, K. Baur, K. Richter, H.J. Rziha, and P. Staeheli. 2005. CD8 T cells require gamma interferon to clear borna disease virus from the brain and prevent immune system-mediated neuronal damage. *J. Virol.* 79:13509–13518. https://doi.org/10.1128/JVI.79.21.13509-13518.2005

Haybaeck, J., N. Zeller, M.J. Wolf, A. Weber, U. Wagner, M.O. Kurrer, J. Bremer, G. Iezzi, R. Graf, P.-A. Clavien, et al. 2009. A lymphotoxin-driven pathway to hepatocellular carcinoma. *Cancer Cell.* 16:295–308. https://doi.org/10.1016/j.ccr.2009.08.021

Heaton, N.S., R.A. Langlois, D. Sachs, J.K. Lim, P. Palese, and B.R. tenOever. 2014. Long-term survival of influenza virus infected club cells drives immunopathology. *J. Exp. Med.* 211:1707–1714. https://doi.org/10.1084/jem.20140488

Hermant, P., C. Demarez, T. Mahlakõiv, P. Staeheli, P. Meuleman, and T. Michiels. 2014. Human but not mouse hepatocytes respond to interferon-lambda in vivo. *PLoS One.* 9:e87906. https://doi.org/10.1371/journal.pone.0087906

Holland, C.H., J. Tanevski, J. Perales-Patón, J. Gleixner, M.P. Kumar, E. Mereu, B.A. Joughin, O. Stegle, D.A. Lauffenburger, H. Heyn, et al. 2020. Robustness and applicability of transcription factor and pathway analysis tools on single-cell RNA-seq data. *Genome Biol.* 21:36. https://doi.org/10.1186/s13059-020-1949-z

Hoshida, Y., A. Villanueva, A. Sangiovanni, M. Sole, C. Hur, K.L. Andersson, R.T. Chung, J. Gould, K. Kojima, S. Gupta, et al. 2013. Prognostic gene expression signature for patients with hepatitis C-related early-stage cirrhosis. *Gastroenterology.* 144:1024–1030. https://doi.org/10.1053/j.gastro.2013.01.021

Hotchin, J. 1962. The biology of lymphocytic choriomeningitis infection: virus-induced immune disease. *Cold Spring Harb. Symp. Quant. Biol.* 27: 479–499. https://doi.org/10.1101/SQB.1962.027.001.046

Hotchin, J. 1973a. Cyclical transient infection, an explanation of persistent virus infection. *In* Lymphocytic Choriomeningitis Virus and Other Arenaviruses: Symposium Held at the Heinrich-Pette-Institut für Experimentelle Virologie und Immunologie, Universität Hamburg, October 16–18, 1972. F. Lehmann-Grube, editor. Springer Berlin Heidelberg, Berlin, Heidelberg. 85–99. https://doi.org/10.1007/978-3-642-65681-1_8

Hotchin, J. 1973b. Transient virus infection: spontaneous recovery mechanism of lymphocytic choriomeningitis virrus-infected cells. *Nat. New Biol.* 241:270–272. https://doi.org/10.1038/newbio241270a0

Hotchin, J. 1974. Cyclical phenomena in persistent virus infection. *J. Reticuloendothel. Soc.* 15:304–311.

Joly, E., L. Mucke, and M.B. Oldstone. 1991. Viral persistence in neurons explained by lack of major histocompatibility class I expression. *Science.* 253:1283–1285. https://doi.org/10.1126/science.1891717

Kallert, S.M., S. Darbre, W.V. Bonilla, M. Kreutzfeldt, N. Page, P. Müller, M. Kreuzaler, M. Lu, S. Favre, F. Kreppel, et al. 2017. Replicating viral vector platform exploits alarmin signals for potent CD8$^+$ T cell-mediated tumour immunotherapy. *Nat. Commun.* 8:15327. https://doi.org/10.1038/ncomms15327

King, B.R., A. Samacoits, P.L. Eisenhauer, C.M. Ziegler, E.A. Bruce, D. Zenklusen, C. Zimmer, F. Mueller, and J. Botten. 2018. Visualization of Arenavirus RNA Species in Individual Cells by Single-Molecule Fluorescence *In Situ* Hybridization Suggests a Model of Cyclical Infection and Clearance during Persistence. *J. Virol.* 92:e02241-17. https://doi.org/10.1128/JVI.02241-17

Kranzusch, P.J., and S.P. Whelan. 2011. Arenavirus Z protein controls viral RNA synthesis by locking a polymerase-promoter complex. *Proc. Natl. Acad. Sci. USA.* 108:19743–19748. https://doi.org/10.1073/pnas.1112742108

Lehmann-Grube, F. 1967. A carrier state of lymphocytic choriomeningitis virus in L cell cultures. *Nature.* 213:770–773. https://doi.org/10.1038/213770a0

Lehmann-Grube, F., U. Assmann, C. Löliger, D. Moskophidis, and J. Löhler. 1985. Mechanism of recovery from acute virus infection. I. Role of T lymphocytes in the clearance of lymphocytic choriomeningitis virus from spleens of mice. *J. Immunol.* 134:608–615.

Liao, Y., G.K. Smyth, and W. Shi. 2014. featureCounts: an efficient general purpose program for assigning sequence reads to genomic features.

Bioinformatics. 30:923–930. https://doi.org/10.1093/bioinformatics/btt656

Lieberman, P.M. 2016. Epigenetics and Genetics of Viral Latency. *Cell Host Microbe.* 19:619–628. https://doi.org/10.1016/j.chom.2016.04.008

Livet, J., T.A. Weissman, H. Kang, R.W. Draft, J. Lu, R.A. Bennis, J.R. Sanes, and J.W. Lichtman. 2007. Transgenic strategies for combinatorial expression of fluorescent proteins in the nervous system. *Nature.* 450: 56–62. https://doi.org/10.1038/nature06293

Luche, H., O. Weber, T. Nageswara Rao, C. Blum, and H.J. Fehling. 2007. Faithful activation of an extra-bright red fluorescent protein in "knock-in" Cre-reporter mice ideally suited for lineage tracing studies. *Eur. J. Immunol.* 37:43–53. https://doi.org/10.1002/eji.200636745

Lucifora, J., Y. Xia, F. Reisinger, K. Zhang, D. Stadler, X. Cheng, M.F. Sprinzl, H. Koppensteiner, Z. Makowska, T. Volz, et al. 2014. Specific and nonhepatotoxic degradation of nuclear hepatitis B virus cccDNA. *Science.* 343:1221–1228. https://doi.org/10.1126/science.1243462

McCarthy, D.J., Y. Chen, and G.K. Smyth. 2012. Differential expression analysis of multifactor RNA-Seq experiments with respect to biological variation. *Nucleic Acids Res.* 40:4288–4297. https://doi.org/10.1093/nar/gks042

Mombaerts, P., J. Iacomini, R.S. Johnson, K. Herrup, S. Tonegawa, and V.E. Papaioannou. 1992. RAG-1-deficient mice have no mature B and T lymphocytes. *Cell.* 68:869–877. https://doi.org/10.1016/0092-8674(92)90030-G

Mosca, J.D., and P.M. Pitha. 1986. Transcriptional and posttranscriptional regulation of exogenous human beta interferon gene in simian cells defective in interferon synthesis. *Mol. Cell. Biol.* 6:2279–2283. https://doi.org/10.1128/MCB.6.6.2279

Moseman, E.A., A.C. Blanchard, D. Nayak, and D.B. McGavern. 2020. T cell engagement of cross-presenting microglia protects the brain from a nasal virus infection. *Sci. Immunol.* 5:eabb1817. https://doi.org/10.1126/sciimmunol.abb1817

Nakagawa, S., L. Wei, W.M. Song, T. Higashi, S. Ghoshal, R.S. Kim, C.B. Bian, S. Yamada, X. Sun, A. Venkatesh, et al. Precision Liver Cancer Prevention Consortium. 2016. Molecular Liver Cancer Prevention in Cirrhosis by Organ Transcriptome Analysis and Lysophosphatidic Acid Pathway Inhibition. *Cancer Cell.* 30:879–890. https://doi.org/10.1016/j.ccell.2016.11.004

Oldstone, M.B.A., and M.J. Buchmeier. 1982. Restricted expression of viral glycoprotein in cells of persistently infected mice. *Nature.* 300:360–362. https://doi.org/10.1038/300360a0

Oldstone, M.B., P. Blount, P.J. Southern, and P.W. Lampert. 1986. Cytoimmunotherapy for persistent virus infection reveals a unique clearance pattern from the central nervous system. *Nature.* 321: 239–243. https://doi.org/10.1038/321239a0

Palliyaguru, D.L., and F. Wu. 2013. Global geographical overlap of aflatoxin and hepatitis C: controlling risk factors for liver cancer worldwide. *Food Addit. Contam. Part A Chem. Anal. Control Expo. Risk Assess.* 30:534–540. https://doi.org/10.1080/19440049.2012.751630

Parra, B., D.R. Hinton, N.W. Marten, C.C. Bergmann, M.T. Lin, C.S. Yang, and S.A. Stohlman. 1999. IFN-γ is required for viral clearance from central nervous system oligodendroglia. *J. Immunol.* 162:1641–1647.

Patterson, C.E., D.M.P. Lawrence, L.A. Echols, and G.F. Rall. 2002. Immune-mediated protection from measles virus-induced central nervous system disease is noncytolytic and gamma interferon dependent. *J. Virol.* 76:4497–4506. https://doi.org/10.1128/JVI.76.9.4497-4506.2002

Pinschewer, D.D., L. Flatz, R. Steinborn, E. Horvath, M. Fernandez, H. Lutz, M. Suter, and A. Bergthaler. 2010. Innate and adaptive immune control of genetically engineered live-attenuated arenavirus vaccine prototypes. *Int. Immunol.* 22:749–756. https://doi.org/10.1093/intimm/dxq061

Pircher, H., K. Bürki, R. Lang, H. Hengartner, and R.M. Zinkernagel. 1989. Tolerance induction in double specific T-cell receptor transgenic mice varies with antigen. *Nature.* 342:559–561. https://doi.org/10.1038/342559a0

Planz, O., S. Ehl, E. Furrer, E. Horvath, M.-A. Bründler, H. Hengartner, and R.M. Zinkernagel. 1997. A critical role for neutralizing-antibody-producing B cells, CD4(+) T cells, and interferons in persistent and acute infections of mice with lymphocytic choriomeningitis virus: implications for adoptive immunotherapy of virus carriers. *Proc. Natl. Acad. Sci. USA.* 94:6874–6879. https://doi.org/10.1073/pnas.94.13.6874

Reuther, P., K. Göpfert, A.H. Dudek, M. Heiner, S. Herold, and M. Schwemmle. 2015. Generation of a variety of stable Influenza A reporter viruses by genetic engineering of the NS gene segment. *Sci. Rep.* 5:11346. https://doi.org/10.1038/srep11346

Siegrist, C.A. 2001. Neonatal and early life vaccinology. *Vaccine.* 19:3331–3346. https://doi.org/10.1016/S0264-410X(01)00028-7

Srinivas, S., T. Watanabe, C.-S. Lin, C.M. William, Y. Tanabe, T.M. Jessell, and F. Costantini. 2001. Cre reporter strains produced by targeted insertion of EYFP and ECFP into the ROSA26 locus. *BMC Dev. Biol.* 1:4. https://doi.org/10.1186/1471-213X-1-4

Steinbach, K., I. Vincenti, K. Egervari, M. Kreutzfeldt, F. van der Meer, N. Page, B. Klimek, I. Rossitto-Borlat, G. Di Liberto, A. Muschaweckh, et al. 2019. Brain-resident memory T cells generated early in life predispose to autoimmune disease in mice. *Sci. Transl. Med.* 11:eaav5519. https://doi.org/10.1126/scitranslmed.aav5519

Thimme, R. 2021. T cell immunity to hepatitis C virus: Lessons for a prophylactic vaccine. *J. Hepatol.* 74:220–229. https://doi.org/10.1016/j.jhep.2020.09.022

Thimme, R., S. Wieland, C. Steiger, J. Ghrayeb, K.A. Reimann, R.H. Purcell, and F.V. Chisari. 2003. CD8(+) T cells mediate viral clearance and disease pathogenesis during acute hepatitis B virus infection. *J. Virol.* 77: 68–76. https://doi.org/10.1128/JVI.77.1.68-76.2003

Thoms, J.A., Y. Birger, S. Foster, K. Knezevic, Y. Kirschenbaum, V. Chandrakanthan, G. Jonquieres, D. Spensberger, J.W. Wong, S.H. Oram, et al. 2011. ERG promotes T-acute lymphoblastic leukemia and is transcriptionally regulated in leukemic cells by a stem cell enhancer. *Blood.* 117: 7079–7089. https://doi.org/10.1182/blood-2010-12-317990

Tishon, A., M. Eddleston, J.C. de la Torre, and M.B.A. Oldstone. 1993. Cytotoxic T lymphocytes cleanse viral gene products from individually infected neurons and lymphocytes in mice persistently infected with lymphocytic choriomeningitis virus. *Virology.* 197:463–467. https://doi.org/10.1006/viro.1993.1613

Tishon, A., H. Lewicki, G. Rall, M. Von Herrath, and M.B.A. Oldstone. 1995. An essential role for type 1 interferon-γ in terminating persistent viral infection. *Virology.* 212:244–250. https://doi.org/10.1006/viro.1995.1477

Traub, E. 1936. The Epidemiology of Lymphocytic Choriomeningitis in White Mice. *J. Exp. Med.* 64:183–200. https://doi.org/10.1084/jem.64.2.183

Varho, M., F. Lehmann Grube, and M.M. Simon. 1981. Effector T lymphocytes in lymphocytic choriomeningitis virus-infected mice. Cytolytic activity of Lyt-23 spleen cells in vitro does not correlate with elimination of infectious virus from spleens. *J. Exp. Med.* 153:992–997. https://doi.org/10.1084/jem.153.4.992

Volkert, M. 1963. STUDIES ON IMMUNOLOGICAL TOLERANCE TO LCM VIRUS. 2. TREATMENT OF VIRUS CARRIER MICE BY ADOPTIVE IMMUNIZATION. *Acta Pathol. Microbiol. Scand.* 57:465–487. https://doi.org/10.1111/j.1699-0463.1963.tb05115.x

Volkert, M., and C. Lundstedt. 1968. The provocation of latent lymphocytic choriomeningitis virus infections in mice by treatment with antilymphocytic serum. *J. Exp. Med.* 127:327–339. https://doi.org/10.1084/jem.127.2.327

Ware, C.F. 2005. Network communications: lymphotoxins, LIGHT, and TNF. *Annu. Rev. Immunol.* 23:787–819. https://doi.org/10.1146/annurev.immunol.23.021704.115719

Weber, C., L. Martínez Peralta, and F. Lehmann-Grube. 1983. Persistent infection of cultivated cells with lymphocytic choriomeningitis virus: regulation of virus replication. Brief report. *Arch. Virol.* 77:271–276. https://doi.org/10.1007/BF01309275

Welsh, R.M., and C.J. Pfau. 1972. Determinants of lymphocytic choriomeningitis interference. *J. Gen. Virol.* 14:177–187. https://doi.org/10.1099/0022-1317-14-2-177

Wohlfahrt, T., S. Rauber, S. Uebe, M. Luber, A. Soare, A. Ekici, S. Weber, A.-E. Matei, C.-W. Chen, C. Maier, et al. 2019. PU.1 controls fibroblast polarization and tissue fibrosis. *Nature.* 566:344–349. https://doi.org/10.1038/s41586-019-0896-x

Zaza, A.D., C.H. Herbreteau, C.N. Peyrefitte, and S.F. Emonet. 2018. Mammarenaviruses deleted from their Z gene are replicative and produce an infectious progeny in BHK-21 cells. *Virology.* 518:34–44. https://doi.org/10.1016/j.virol.2018.01.013

Zinkernagel, R.M. 2002. Lymphocytic choriomeningitis virus and immunology. *Curr. Top. Microbiol. Immunol.* 263:1–5.

Supplemental material

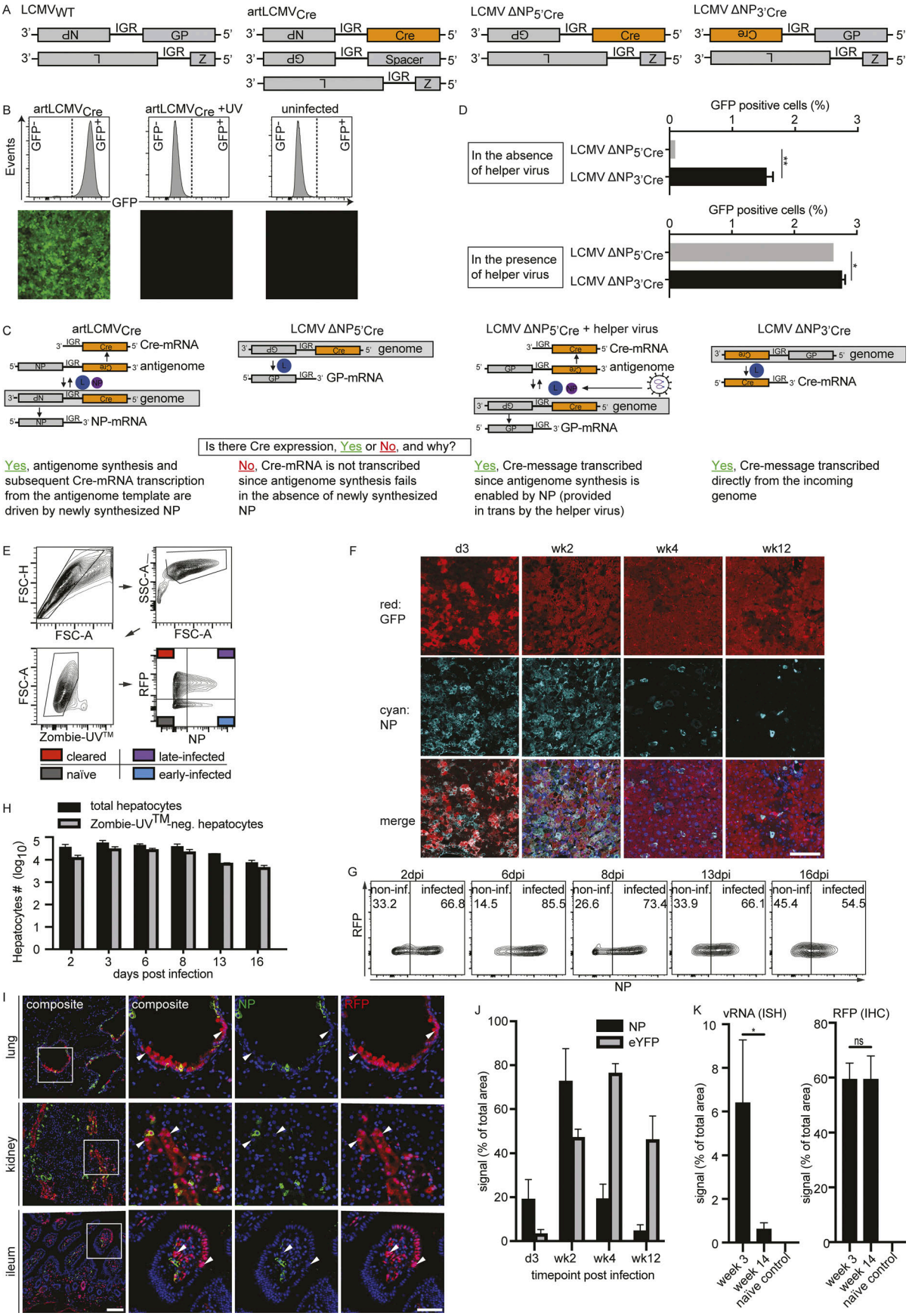
A
LCMV$_{WT}$
artLCMV$_{Cre}$
LCMV ΔNP$_{5'Cre}$
LCMV ΔNP$_{3'Cre}$
B
artLCMV$_{Cre}$
artLCMV$_{Cre}$ +UV
uninfected
Events
GFP
D
GFP positive cells (%)
In the absence of helper virus
In the presence of helper virus
LCMV ΔNP$_{5'Cre}$
LCMV ΔNP$_{3'Cre}$
C
artLCMV$_{Cre}$
LCMV ΔNP$_{5'Cre}$
LCMV ΔNP$_{5'Cre}$ + helper virus
LCMV ΔNP$_{3'Cre}$
Cre-mRNA
antigenome
genome
NP-mRNA
GP-mRNA
Is there Cre expression, Yes or No, and why?
Yes, antigenome synthesis and subsequent Cre-mRNA transcription from the antigenome template are driven by newly synthesized NP
No, Cre-mRNA is not transcribed since antigenome synthesis fails in the absence of newly synthesized NP
Yes, Cre-message transcribed since antigenome synthesis is enabled by NP (provided in trans by the helper virus)
Yes, Cre-message transcribed directly from the incoming genome
E
FSC-H
FSC-A
SSC-A
Zombie-UV™
RFP
NP
cleared
late-infected
naïve
early-infected
F
d3
wk2
wk4
wk12
red: GFP
cyan: NP
merge
G
2dpi
6dpi
8dpi
13dpi
16dpi
non-inf.
infected
33.2
66.8
14.5
85.5
26.6
73.4
33.9
66.1
45.4
54.5
RFP
NP
H
total hepatocytes
Zombie-UV™-neg. hepatocytes
Hepatocytes # (log_{10})
days post infection
I
composite
NP
RFP
lung
kidney
ileum
J
NP
eYFP
signal (% of total area)
timepoint post infection
K
vRNA (ISH)
RFP (IHC)
ns
week 3
week 14
naive control

Figure S1. **Evaluation of artLCMV$_{Cre}$ as a tool to induce Cre recombination exclusively in cells replicating the viral genome (related to Figs. 1, 2, 3, 4, and 5) and the analysis of LCMV-infected mouse hepatocytes in vivo and in cell culture and the occurrence of cleared cells in lung, kidney and ileum (related to Fig. 1). (A)** Genome organization of WT LCMV (LCMV$_{WT}$) and the respective Cre-encoding viruses used for this figure. For artLCMV$_{Cre}$, a spacer gene encoding an irrelevant protein, in this example tomato, is encoded in cis with the GP. **(B)** Flow-cytometric quantification and fluorescent live cell imaging of GFP-reporting A549$_{floxGFP}$ cells 48 h after infection with artLCMV$_{Cre}$, UV-treated artLCMV$_{Cre}$ (both at MOI = 0.1), or mock. The resulting pattern of GFP expression excludes cell-to-cell transfer of functional Cre protein by (otherwise defective) viral particles. **(C)** Schematic representation of the transcription and/or replication steps the Cre-encoding S segments of artLCMV$_{Cre}$ and of the NP-deficient viruses LCMVΔNP$_{5'Cre}$ and LCMVΔNP$_{3'Cre}$, respectively, can undergo in the absence of helper virus. Synthesis of antigenomic RNA using the incoming viral S segment RNA (gray boxes) as a template requires de novo expression of NP (purple) and L (blue). Henceforth, LCMVΔNP$_{5'Cre}$ is not predicted to express Cre-mRNA (and protein) unless NP is provided in trans by a helper virus, which restores antigenome synthesis. **(D)** We infected A549$_{floxGFP}$ cells with LCMVΔNP$_{5'Cre}$ or LCMVΔNP$_{3'Cre}$ (MOI = 0.01) in the presence or absence of a LCMVΔGP helper virus (MOI = 1). 48 h later, we quantified the frequency (percent) of Cre-recombined (GFP-expressing) cells. The result from this experiment demonstrates that the sole presence of viral RNA encoding Cre under control of the 5′ untranslated region, as it is encoded in artLCMV$_{Cre}$, does not allow for Cre-expression. This finding excluded Cre-reporting in abortively infected cells, i.e., in cells not supporting viral antigenome replication and subsequent mRNA transcription from the newly synthesized template. Error bars represent the SD of three independent culture wells. Unpaired two-tailed Student's *t* test was used for pairwise comparisons. *, P < 0.05; **, P < 0.01 (D). Representative data from two similar, independently conducted experiments are shown (B and D). **(E)** Gating strategy for the flow-cytometric analysis of NP expression and Cre-reporting by murine hepatocytes. We infected neonatal STOP$_{flox}$-RFP mice with artLCMV$_{Cre}$. Hepatocytes were isolated 5 wk later and subjected to flow-cytometric analysis. **(F)** Fluorescent costaining of viral NP and Cre-induced eYFP in liver sections of STOP$_{flox}$eYFP mice neonatally infected with artLCMV$_{Cre}$ (scale bar, 100 µm). One representative of several areas analyzed in at least three mice per time point is shown. **(G)** We isolated and cultured primary hepatocytes of STOP$_{flox}$RFP mice. At the indicated time points after infection with WT LCMV (MOI = 0.1), we analyzed viral NP expression. Numbers within the plots indicate percentages of NP-negative cells (left gates) and NP-positive cells (right gates). Representative FACS plots of two independent experiments are shown. **(H)** Total numbers of primary hepatocytes of STOP$_{flox}$RFP mice (black columns) as analyzed in the experiment to Fig. 1 A. Time points after infection with artLCMV$_{Cre}$ (MOI = 0.025) are indicated. Gray columns indicate the number of viable hepatocytes in these cultures as judged by a lack of Zombie UV incorporation. One representative of two independently conducted experiments is shown. **(I)** Fluorescent costaining of viral NP (green) and Cre-induced RFP (red) in sections of the indicated organs of 12-wk-old STOP$_{flox}$RFP mice neonatally infected with artLCMV$_{Cre.}$ Arrowheads point out select noncytolytically cleared cells (left scale bar, 100 µm; right scale bar, 50 µm). One representative of several areas analyzed in five mice is shown. **(J)** Quantification of NP and eYFP staining in the liver sections of artLCMV$_{Cre}$-infected STOP$_{flox}$eYFP mice (*n* = 3) presented in Fig. 1 E. Time points after neonatal infection are indicated. **(K)** Quantification of the area stained by in situ hybridization (ISH) of viral RNA (vRNA, left) and by anti-RFP antibody (right) in the liver sections of artLCMV$_{Cre}$-infected STOP$_{flox}$RFP mice (*n* = 3) reported in Fig. 1 F. Time points after neonatal infection are indicated. Error bars represent SEM. Unpaired two-tailed Student's *t* test was used on log-converted values for pairwise comparisons. *, P < 0.05. dpi, days post-infection; FSC-H, forward scatter height; FSC-A, forward scatter area; IGR, intergenic region; neg., negative; non-inf., non-infected; SSC-A, sideward scatter area.

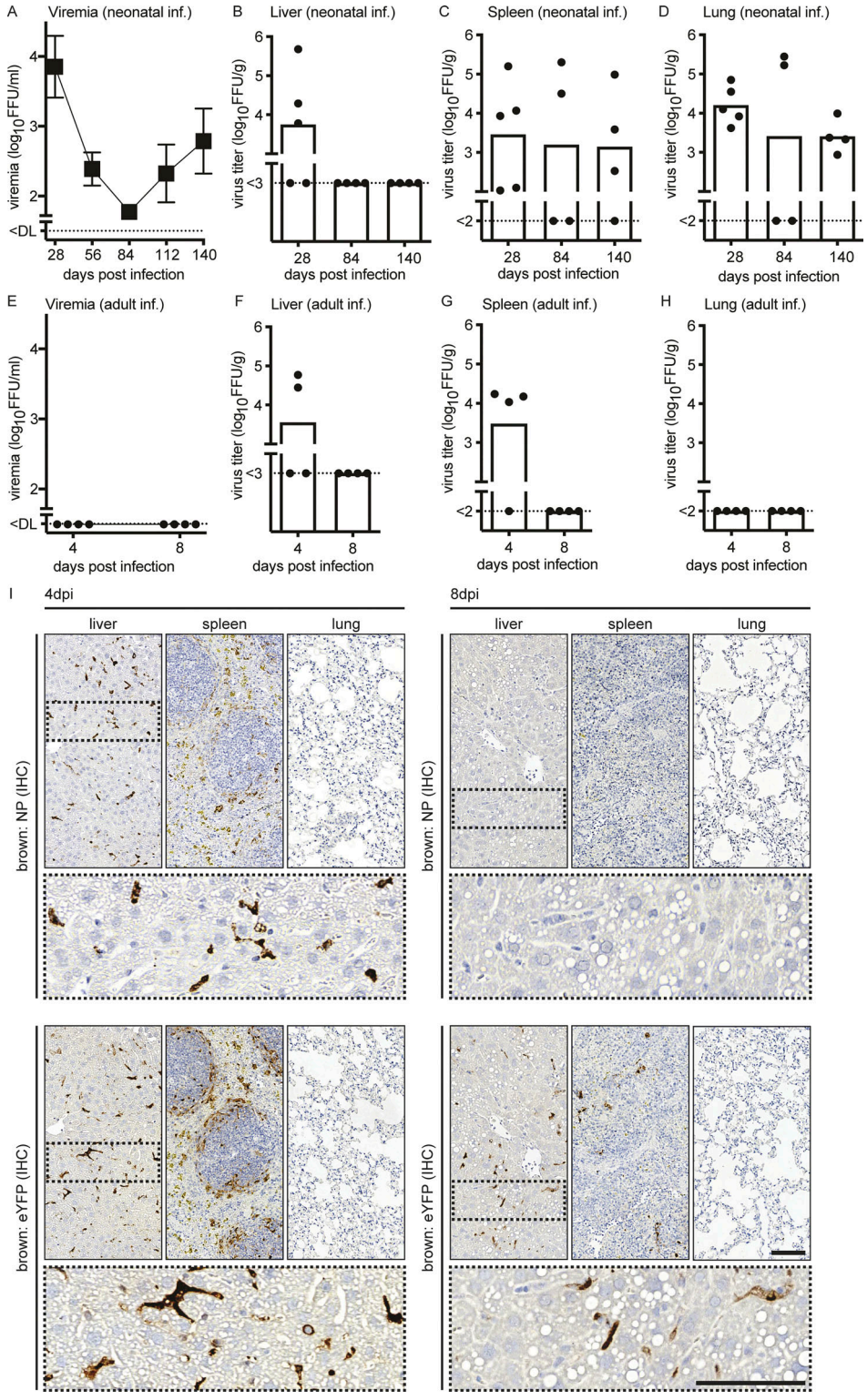

Figure S2. **Analysis of viral replication in mice infected neonatally or at adult age with artLCMV$_{Cre}$ (related to Fig. 1). (A and E)** Viremia of STOP$_{flox}$eYFP mice infected neonatally (A) or at adult age (E) with artLCMV$_{Cre}$ at the indicated time points after infection. **(B–D and F–H)** Viral titer in the indicated organs of STOP$_{flox}$eYFP mice infected neonatally (B–D) or at adult age (F–H) with artLCMV$_{Cre}$. Organ-specific detection limits are due to differential cytotoxicity of the respective homogenates (B–D and F–H). **(I)** Immunohistochemical analysis of NP and eYFP expression in spleen, liver, and lung sections of STOP$_{flox}$eYFP mice infected at an adult age with artLCMVCre and collected either 4 or 8 d later (scale bars, 100 µm). In the liver, artLCMV$_{Cre}$ infection is restricted to Kupffer cells, which are distinguishable from (uninfected) hepatocytes by their shape and size. Representative images from one out of four animals are shown (same animals as in F–H). One representative of two similar experiments is shown in A–H. One representative liver area (I) out of 23 similarly sized areas is analyzed from four individual mice. DL, detection limit; dpi, days post-infection; FFU, focus forming units; inf., infection; IHC, immunohistochemistry.

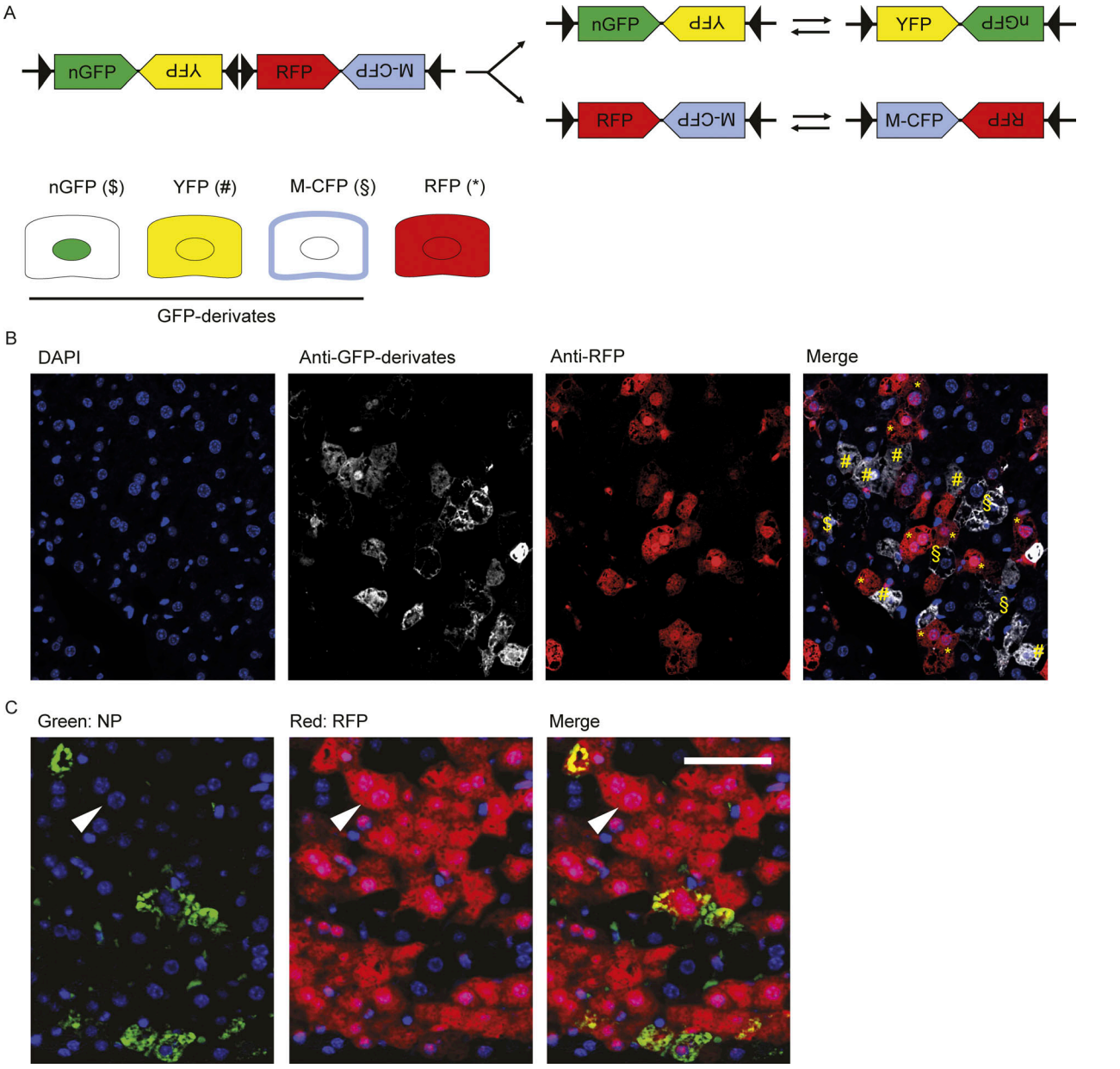

Figure S3. **Clonality fate mapping of virus-cleared mouse hepatocytes in vivo (related to Fig. 1) and visualization of noncytolytically cleared hepatocytes of RAG-1–deficient mice (related to Fig. 2). (A and B)** We infected neonatal R26R-Confetti mice (n = 3) with artLCMV$_{Cre}$. **(A)** These animals stochastically express one out of four fluorescent proteins upon Cre-recombination: nuclear GFP (nGFP, $), YFP (#), membrane-associated CFP (M-CFP, §) or RFP (*). **(B)** We collected liver sections at week 12 after neonatal infection and performed a fluorescent costaining combining an antibody detecting the three GFP-derivates (nGFP, YFP, and M-CFP) with a second antibody directed against RFP. GFP-derivates are distinguishable by their subcellular localization. The image shows a representative liver area with several small clusters of Cre-recombined (fluorescent) hepatocytes. One representative liver area out of 14 similarly sized areas analyzed from three mice. **(C)** Fluorescent costaining of viral NP (green) and Cre-induced RFP (red) in liver sections of 4-wk-old Rag-1 × STOP$_{flox}$RFP mice neonatally infected with artLCMV$_{Cre}$. The arrowheads point to one out of several noncytolytically cleared cells in this visual field (scale bar, 50 µm). One representative liver area out of 14 similarly sized areas from three mice is shown.

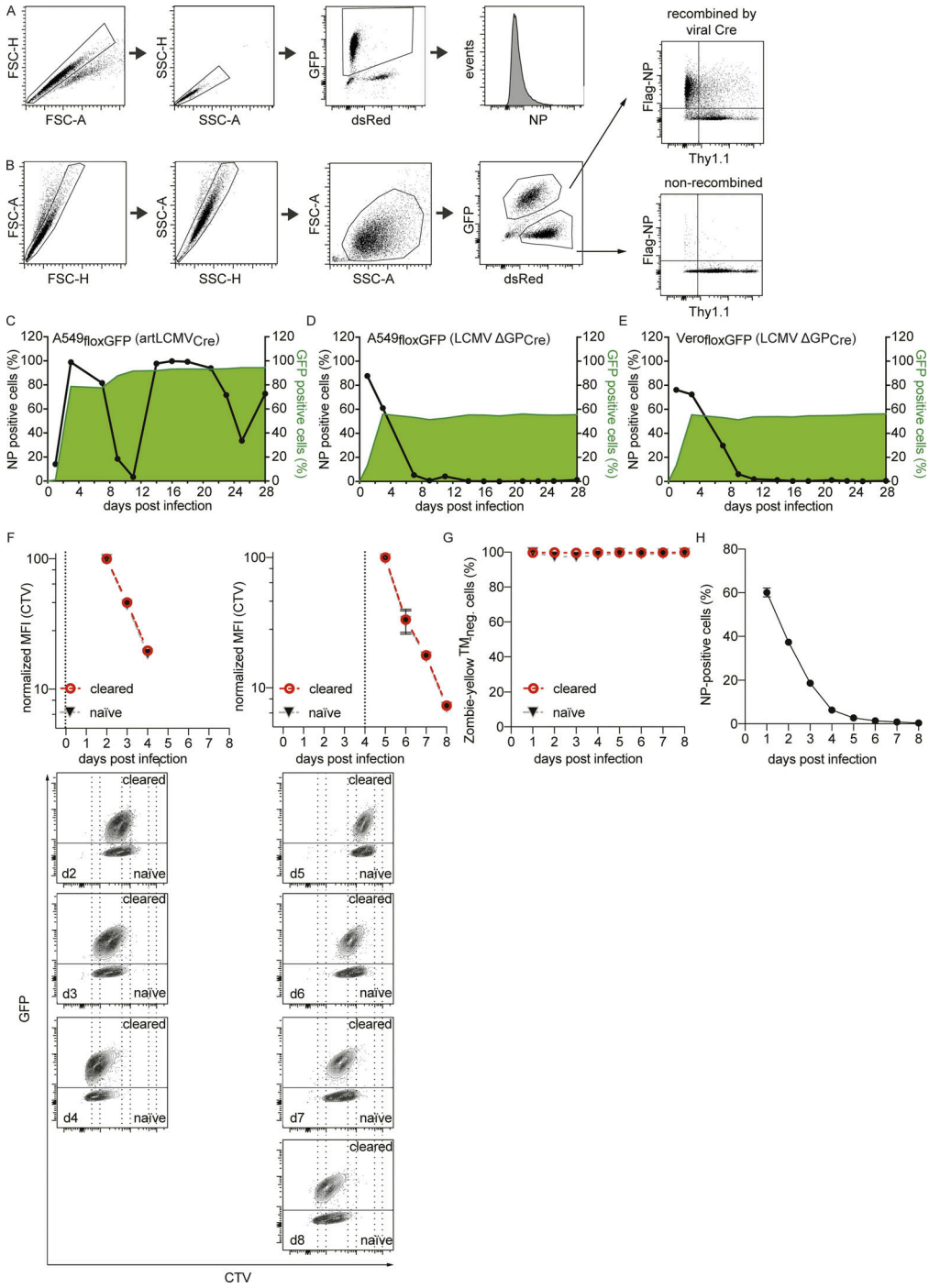

Figure S4. **Gating strategy to detect GFP–, Thy1.1–, and NP-Flag–expressing cells, and characterization of cultured cells cleared from infection (related to Fig. 3). (A and B)** Gating strategy for flow-cytometric analysis of Cre-reporting $A549_{floxGFP}$ cells infected with LCMV expressing untagged NP (A) or N-terminally flag-tagged NP (B). **(C–E)** Alternative analysis of the data represented in Fig. 3, A, B, and D. Unlike in the aforementioned main figure panels reporting the MFI from the same datasets, viral NP and also GFP expression are plotted as a percentage of all $A549_{flox}$GFP cells (C and D) and $Vero_{flox}$GFP cells (E) in the respective cultures. Cells were infected with $artLCMV_{Cre}$ (MOI = 0.01; C) or $LCMV\Delta GP_{Cre}$ (MOI = 0.5; D and E). xy plots are representative of six replicates (C–E). **(F and G)** Proliferation (F) and viability (G) of cleared (GFP^+, NP^-) cells as compared with naive (GFP^-, NP^-) cells within an $LCMV\Delta GP_{Cre}$-infected (MOI = 0.5) $A549_{floxGFP}$ culture. Cells were labeled with CellTrace Violet (CTV) on day 0 (F, left) or on day 4 after infection (F, right) and the dilution of the dye was determined over time as a surrogate of cell proliferation. The MFI of CTV was normalized to the one of naive cells on day 2 (F, left) and day 5 (F, right), respectively. Exemplary contour plots at the bottom of each panel show representative CTV stains (n = 3) of cleared cells (GFP^+, NP^-) and naive cells (GFP^-, NP^-) at the indicated time points after infection. The percentage of viable cells among the cleared and naive population was determined by Zombie Yellow staining (G). **(H)** Quantification of viral NP-expressing cells within the same $LCMV\Delta GP_{Cre}$-infected $A549_{floxGFP}$ cultures analyzed in F and G. Error bars represent the SD of three independently infected cultures. Two independent experiments were conducted to analyze cells on days 2–4 and days 5–8 after infection, respectively (F–H). FSC-H, forward scatter height; FSC-A, forward scatter area; MFI, mean fluorescence intensity; neg., negative; SSC-A; sideward scatter area; SSC-A, sideward scatter height.

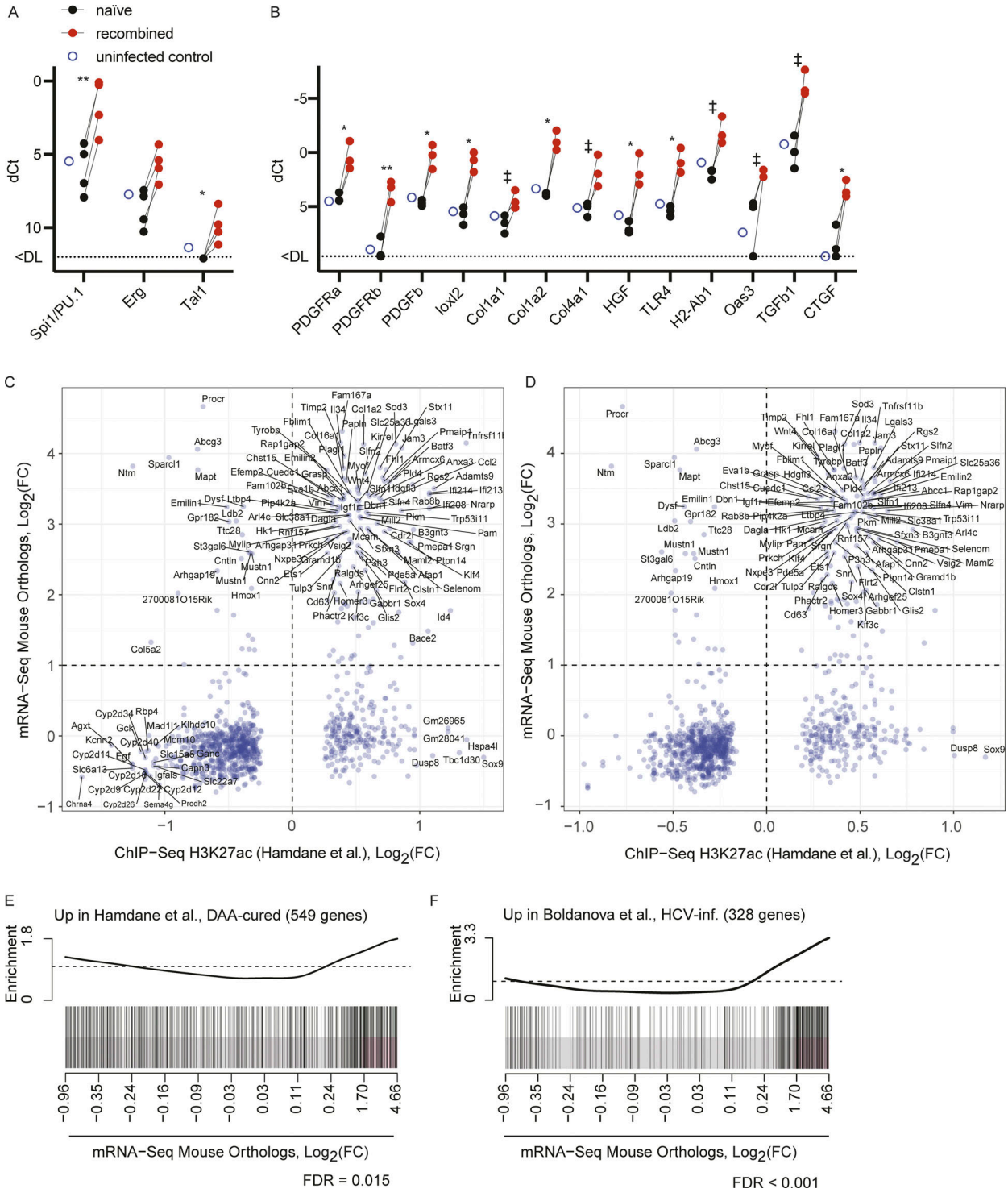

Figure S5. **Validation of differentially expressed genes and comparison of LCMV transcriptomic footprint to HCV-cured and -infected patients (related to Fig. 5). (A and B)** We infected neonatal STOP$_{flox}$RFP mice to collect RFP-positive and RFP-negative hepatocytes 14 wk later (analogously to Fig. 5, A–D but independent experiments). We performed TaqMan RT-PCR to validate the differential expression of the TFs Spi1/PU.1, Erg, and Tal1 (A) and additional selected genes emerging from the experiment in Fig. 5, A–D (B). Expression levels were normalized to GAPDH. **(A and B)** Two independent experiments. Hepatocytes from uninfected STOP$_{flox}$RFP mice served as negative control (n = 3 [mean, A] or n = 1 [B]). Paired two-tailed Student's t test was used for pairwise comparisons. ‡, P < 0.1; *, P < 0.05; **, P < 0.01. Representative data from two similar, independently conducted experiments are shown (A). **(C and D)** Scatter plot comparing H3K27ac changes observed by Hamdane et al. (2019) in DAA-cured patients (group 1; C) or HCV-infected patients (D) to RNA levels of the respective mouse orthologs emerging from this study (Fig. 5, A–D). **(E and F)** Enrichment analysis of genes found to be up-regulated (Log$_2$[FC] > 1) by mRNA-Seq in DAA-cured patients (E; Hamdane et al., 2019) and HCV-infected patients (F; Boldanova et al., 2017) having a mouse ortholog among the regulated mouse genes (RFP$^+$ versus RFP$^-$ in Fig. 5, A–D) emerging from this study. ChIP-seq, chromatin immunoprecipitation DNA-sequencing; DL, detection limit; inf., infected.

Table S1 is provided online as a separate file and shows a comparison of H3K27ac changes observed in HCV-infected or DAA-cured patients with changes of mRNA levels between RFP-positive and RFP-negative hepatocytes of mice neonatally infected with artLCMV$_{Cre}$.